Coexistence of enriched and modern-like 142 Nd signatures in Archean igneous rocks of the eastern Kaapvaal Craton, southern Africa

Kathrin P. Schneider, J. Elis Hoffmann, Maud Boyet, Carsten Münker, Alfred Kröner

▶ **To cite this version:**

Kathrin P. Schneider, J. Elis Hoffmann, Maud Boyet, Carsten Münker, Alfred Kröner. Coexistence of enriched and modern-like 142 Nd signatures in Archean igneous rocks of the eastern Kaapvaal Craton, southern Africa. Earth and Planetary Science Letters, 2018, 487, pp.54-66. 10.1016/j.epsl.2018.01.022 . hal-01723662

HAL Id: hal-01723662
https://uca.hal.science/hal-01723662

Submitted on 5 Mar 2018

HAL is a multi-disciplinary open access archive for the deposit and dissemination of scientific research documents, whether they are published or not. The documents may come from teaching and research institutions in France or abroad, or from public or private research centers.

L'archive ouverte pluridisciplinaire **HAL**, est destinée au dépôt et à la diffusion de documents scientifiques de niveau recherche, publiés ou non, émanant des établissements d'enseignement et de recherche français ou étrangers, des laboratoires publics ou privés.

Coexistence of enriched and modern-like ^{142}Nd signatures in Archean igneous rocks of the eastern Kaapvaal Craton, southern Africa

Kathrin P. Schneider[1], J. Elis Hoffmann[1], Maud Boyet[2], Carsten Münker[3], Alfred Kröner[4]

[1]Institut für Geologische Wissenschaften, Freie Universität Berlin, Germany (*kathrin.schneider@fu-berlin.de)

[2]Laboratoire Magmas et Volcans, Université Clermont Auvergne, France

[3]Institut für Geologie und Mineralogie, Universität zu Köln, Germany

[4]Beijing SHRIMP Center, Institute of Geology, Chinese Academy of Geological Sciences, Beijing, China, and Institut für Geowissenschaften, Universität Mainz, Germany

Keywords

^{142}Nd

Kaapvaal Craton

Barberton

Ancient Gneiss Complex

Hadean

Differentiation

Abstract

The short-lived ^{146}Sm-^{142}Nd isotope system is an important tool for tracing Hadean crust-mantle differentiation processes and constraining their imprint on much younger rocks from Archean cratons. We report the first comprehensive set of high-precision ^{142}Nd analyses for granitoids and amphibolites of the Ancient Gneiss Complex (AGC; Swaziland) and the oldest metavolcanic units of the Barberton Greenstone Belt (BGB; South Africa). The investigated samples span an age range from

3.66 Ga to 3.22 Ga and are representative of major geological units of the AGC and the lower Onverwacht Group of the BGB. Measured samples yielded μ^{142}Nd values in the range from -8 ppm to +3 ppm relative to the JNdi-1 terrestrial standard, with typical errors smaller than 4.4 ppm. The distribution of the μ^{142}Nd values for these 17 measured samples is bimodal with ten samples showing a tendency towards slightly negative μ^{142}Nd anomalies, whereas seven samples have ^{142}Nd similar to the terrestrial reference. The only confidently resolvable μ^{142}Nd anomalies were found in a 3.44 Ga Ngwane Gneiss sample and in amphibolites of the ca. 3.45 Ga Dwalile Greenstone Remnant, revealing μ^{142}Nd values ranging from -7.9 ± 4.4 to -6.1 ± 4.3 ppm. The μ^{142}Nd deficits do not correlate with age, lithological unit, or sample locality. Instead, our results reveal that two distinct mantle domains were involved in the formation of the AGC crust. The two reservoirs can be distinguished by their μ^{142}Nd signatures. Mantle-derived rocks tapped the enriched reservoir with negative μ^{142}Nd at least until 3.46 Ga, whereas the granitoids preserved a negative μ^{142}Nd signature that formed by incorporation of older AGC crust at least until 3.22 Ga. The oldest gneisses with no μ^{142}Nd anomaly are up to 3.64 Ga in age, indicating that a modern terrestrial ^{142}Nd reservoir was already present by early Archean times.

1. Introduction

Studying the first billion years of Earth´s evolution is crucial for understanding the early mantle and crustal differentiation history as well as crustal recycling processes. However, the lack of preservation of the Hadean (4.5-4.0 Ga) rock record hinders a direct study of early geodynamic processes. The earliest relicts of potential continental crustal origin are zircon detrital grains from the ca. 3.3 Ga Jack Hills metaquartzites in NW Australia, dating back to almost 4.4 Ga (e.g., Wilde et al. 2001). Metamorphosed felsic continental crust of Eo- and Paleoarchean age (4.0-3.2 Ga) is preserved as grey gneiss terranes in all cratonic nuclei. These predominantly consist of multiphase grey gneisses that comprise juvenile tonalite-trondhjemite-granodiorites (TTGs) and granitoids of various composition, depending on the exposed crustal level and pre-deformation history (e.g., Nutman et al. 1996; Moyen 2011; Anhaeusser 2014; Hoffmann and Kröner, in press). Associated with the granitoids s.l. are greenstone belts, consisting of ultramafic, mafic and felsic volcanic rocks, and their plutonic

equivalents, as well as metasedimentary units. Often, only fragments of the original greenstone associations of various sizes are interlayered with the grey gneisses.

Currently it is under debate in which tectonic environment the early continental crust on Earth formed and stabilized (e.g., van Kranendonk, et al., 2014; Hoffmann et al. 2016 and references therein). Models invoke an initial phase of TTG formation, followed by reworking caused by collision between crustal terranes and involvement of mantle-derived magmas by intrusion and underplating. This led to formation of various types of granitoids that were subsequently strongly deformed and migmatized during post-magmatic metamorphic events. The most prominent relicts of early crustal terranes are the Acasta Gneiss Complex, the Nuvvuagittuq region, the Hudson Bay terrane, and the Eoarchean Labrador gneiss terranes of Canada, as well as the Itsaq Gneiss Complex of southern West Greenland, the Pilbara and northwestern Yilgarn Cratons of Australia, and the Ancient Gneiss Complex located in the eastern Kaapvaal Craton of southern Africa (e.g., Bennett et al. 2007; Van Kranendonk et al. 2007; Roth et al. 2013, 2014a; Kröner et al. 2014; O´Neil and Carlson 2017; and references therein).

One key observation concerning early crust formation is the lack of Hadean (pre-4.0 Ga) crust in Archean terranes, raising the question whether such a protocrust was involved in the formation of Archean terranes or not (e.g., Kemp et al. 2010; Zeh et al. 2011; O'Neil et al. 2013; O'Neil and Carlson 2017). However, the Hadean age of ~4.3 Ga proposed for the Ujaraaluk unit in the Nuvvuagittuq greenstone belt suggests that portions of protocrust survived since its formation (O'Neil et al. 2008). Moreover, based on Hf isotope compositions in zircons, reworking of a Hadean or Eoarchean protocrust has been proposed for different terranes (e.g., Iizuka et al. 2007; Kemp et al. 2010; Zeh et al. 2011; Kröner et al. 2014).

A powerful tool to test the involvement of Hadean crustal sources in the formation of Archean cratonic crust is the short-lived ^{146}Sm-^{142}Nd ($T_{1/2}$ = 103 Ma ± 5 Ma, Meissner et al. 1987) decay system. Due to its short half-life, the ^{146}Sm-^{142}Nd decay system was only active in the first ca. 500 million years of Earth´s evolution. Consequently, differentiation of crustal material from a mantle or crustal source before the extinction of ^{146}Sm will fractionate Sm and Nd because of the slightly more incompatible behavior of Nd compared to Sm during mantle and crustal melting, resulting in

heterogeneities in the $^{142}Nd/^{144}Nd$ composition of early differentiated terrestrial reservoirs (e.g., Harper and Jacobsen 1992; Boyet et al. 2005; Caro et al. 2006; Rizo et al. 2012). During early crust-mantle differentiation, the continental crust developed towards low Sm/Nd isotope ratios, expressed as negative $\mu^{142}Nd$ ($\mu^{142}Nd = (^{142}Nd/^{144}Nd_{sample} / {}^{142}Nd/^{144}Nd_{standard} - 1) \times 10^6$ in ppm) and the depleted mantle developed with a high Sm/Nd isotope ratio, resulting in positive $\mu^{142}Nd$ values. Hence, an offset in $\mu^{142}Nd$ relative to younger rocks can be ascribed to early terrestrial fractionation. Such early terrestrial fractionation events may have included early magma ocean fractionation involving deep mantle phases such as bridgmanite and Ca-perovskite (Corgne et al. 2005) that would directly imprint on the ^{142}Nd composition of the mantle, leaving behind early ^{142}Nd enriched and depleted reservoirs (Boyet et al. 2005; Boyet and Carlson 2006; Caro et al. 2005, 2006). Furthermore, the formation of Hadean mafic crust and residual mantle is mirrored by the ^{142}Nd signature of Archean rocks (O'Neil et al. 2008).

So far, all terrestrial rocks younger than 2.70 Ga were found to have a uniform $^{142}Nd/^{144}Nd$ isotopic composition with $\mu^{142}Nd$ of approximately 0 ± 5 ppm (e.g. Boyet and Carlson 2006; Caro et al. 2006; Roth et al. 2014b). In contrast, some ancient terrains show both positive and negative derivations in $\mu^{142}Nd$ compared to the terrestrial average value for post-Archean rocks.

Positive $\mu^{142}Nd$ anomalies relative to the terrestrial standard have been reported for rocks of the early crustal terranes of Greenland, yielding maximum values of up to +20 ppm (e.g., Boyet and Carlson 2006; Caro et al. 2006; Bennett et al. 2007; Rizo et al. 2011, 2012, 2013; O´Neil et al. 2016). These $\mu^{142}Nd$ anomalies were interpreted to directly trace a Hadean mantle reservoir that differentiated between 4.32 Gyr and 4.51 Gyr ago. Complementary reservoirs with negative $\mu^{142}Nd$ were reported from the Hadean/Eoarchean Nuvvuagittuq Supracrustal Belt (-18 to +8 ppm; O´Neil et al. 2008, 2012; Roth et al. 2013), the 3.40-3.75 Ga Ukalik belt and Innuksuac complex, Canada (-9 to +1 ppm; Caro et al. 2017), the Acasta gneisses, Canada ($\mu^{142}Nd$ as low as -16 ppm; Roth et al. 2014a), as well as from the 3.4-3.5 Ga Ameralik dykes, Greenland (-11 to +16 ppm; Rizo et al. 2012). Similarly, komatiites from the ca. 3.55 Ga Schapenburg Greenstone Remnant (South Africa, Kaapvaal Craton) yielded negative $\mu^{142}Nd$ anomalies as low as -13 ppm and were interpreted to trace material from the crystallization of an early Hadean magma ocean (Puchtel et al. 2016).

Due to the short half-life of the ^{146}Sm-^{142}Nd isotope system, it can be used as a tool for tracing early recycling and mantle stirring processes (Bennett et al. 2007). It has been recognized, that early signatures virtually disappear in magmatic rocks throughout the Archean, with one exception from 2.7 Ga komatiites of the Abitibi belt (Canada) that yielded a μ^{142}Nd anomaly of up to +9 (Debaille et al. 2013). Recently, O'Neil and Carlson (2017) obtained negative μ^{142}Nd anomalies for ca. 2.75 Ga granitoids from the Hudson Bay terrane (Canada), which indicate late Archean reworking of rocks with negative μ^{142}Nd signatures that were derived from ancient reservoirs which initially differentiated from the mantle in the Hadean.

In this study, we focus on Archean granitoids and mantle-derived rocks from the eastern Kaapvaal Craton (South Africa and Swaziland). We report the first high-precision ^{142}Nd/^{144}Nd analyses for well-characterized granitoids and meta-tholeiites (amphibolites) of the Ancient Gneiss Complex (AGC; Swaziland) and from the lower Onverwacht Group of the Barberton Greenstone Belt (BGB; South Africa). The investigated samples span an age range from 3.66 Ga to 3.22 Ga and represent the main lithological units of the AGC and the oldest rocks of the BGB. The data are used to elucidate the differentiation and reworking history of the oldest part of the Kaapvaal Craton. The combination of data derived from the short-lived ^{146}Sm-^{142}Nd system with existing geological, petrological and geochemical information for these samples lead to a deeper understanding of if and how Hadean crustal components were incorporated into the sources of Archean crustal rocks, enabling us to place general constraints on geodynamic processes operating in the early Archean.

2. Geology of the Ancient Gneiss Complex and Barberton Greenstone Belt

The 3.66-3.20 Ga AGC (Hoffmann and Kröner, in press, and references therein) is located in the eastern Kaapvaal Craton and predominantly comprises complexly deformed Paleo- to Mesoarchean grey gneisses of the TTG suite that are interlayered with rare amphibolites (Fig. 1; Hoffmann and Kröner, in press). The 3.66-3.45 Ga Ngwane Gneiss is the oldest component of the AGC (Hoffmann and Kröner, in press, and references therein) and is exposed in central and western Swaziland as well as in the Phophonyane Inlier of northwestern Swaziland. The Ngwane Gneiss

underwent ductile amphibolite- to granulite-facies metamorphism (Kröner et al. 1993, 2014 and references theirein). The interlayered amphibolites represent mafic dykes (Jackson 1984; Hoffmann and Kröner, in press) as well as infolded greenstone remnants (e.g., Jackson 1984; Kröner and Tegtmeyer 1994). The Ngwane Gneiss is intruded by the 3.478-3.430 Ga homogeneous and variously foliated dioritic to tonalitic Tsawela Gneiss (e.g., Jackson 1984; Kröner et al. 1993; Hoffmann et al. 2016), granitoid gneisses of the ca. 3.23 Ga Usutu Intrusive Suite (Schoene et al. 2009), and the 3.1 Ga Pigg´s Peak batholith (Murphy 2015) which divides the AGC from the BGB in the north, as well as several other smaller plutons with ages up to 2.7 Ga (e.g., Zeh et al. 2011). The most prominent and largest supracrustal succession within the AGC is the ca. 3.45 Ga Dwalile Greenstone Remnant (DGR; Kröner and Tegtmeyer 1994) exposed west of Mankanyane town along the border with South Africa.

To the northwest the AGC is tectonically separated from the 3.53-3.20 Ga BGB and surrounding plutons (e.g., Kröner et al. 1991, 1996; Van Kranendonk et al. 2009) by a major faulted contact, the Phophonyane shear zone (Fig. 1). The oldest unit of the BGB is the Onverwacht Group, which comprises mafic and ultramafic volcanic rocks that are interlayered with subordinate felsic volcanic rocks. The BGB is surrounded by several plutons, namely the Steynsdorp, Theespruit, Stolzburg, Nelshoogte, and Kaap Valley plutons with ages of ca. 3.51 to 3.20 Ga. Their compositions range from tonalite to trondhjemite (e.g., Anhaeusser 2014).

The AGC and the southern BGB are characterized by regionally extensive medium-pressure and high-temperature metamorphism that occurred at ca. 3.2 Ga (e.g., Dziggel et al. 2005; Taylor et al. 2012). This metamorphic event led to lower granulite-facies ductile deformation, migmatization, and anatexis, followed by syntectonic emplacement of granitoids in the lower and mid-crustal domains represented by the AGC (e.g., Schoene et al. 2008). In the BGB, this metamorphism caused a greenschist- and upper amphibolite facies overprint, coupled with refolding and structural parallelism between granitoid gneisses and supracrustal rocks (e.g., De Ronde and De Wit 1994; Lowe and Byerly 1999; van Kranendonk et al. 2009, 2014; Kröner et al., 2016).

3. Samples and analytical techniques

168 3.1 Sample selection

169

170 The strategy of our sample selection was to cover a comprehensive range of rocks
171 representative of the early Archean crust of the AGC and BGB that included different lithological
172 units and ages, to gain structural and temporal resolution of possible changes in $^{142}Nd/^{144}Nd$ isotopic
173 compositions. We selected six well-characterized and least altered granitoid gneisses from the AGC,
174 including TTG compositions and grey gneisses of various origins, covering an age range from 3.66 Ga
175 (grey gneiss AGC 150b; Kröner et al. 2014) to 3.22 Ga (grey gneiss AGC 445; age: personal
176 communication A. Kröner 2017). Three of these samples, the 3.66 Ga Ngwane grey gneiss (AGC
177 150b), the 3.55 Ga tonalite from north of Pigg´s Peak town (AGC 370), and the 3.48 Ga tonalitic
178 Tsawela gneiss from west-central Swaziland (AGC 75), reveal heterogeneous Hf-in-zircon isotope
179 compositions implying involvement of older crustal components in the formation of these rocks
180 (Kröner et al. 2014; Hoffmann et al. 2016). Additionally, the 3.26 Ga granodiorite from the Usutu
181 Suite (AGC 368) contains inherited zircons that date back to 3.45 Ga which is in agreement with
182 contribution from an older crustal source (ages: personal communication A. Kröner 2017).
183 Furthermore, two amphibolites and one metagabbro from the AGC were selected, all dating back to
184 ages between >3.40 Ga (AGC 222; Kröner et al. 1993; Taylor et al. 2012; Suhr et al. 2015) and 3.46
185 Ga (AGC 45; Kröner & Tegtmeyer 1994; AGC 350 dated to 3.46 Ga; personal communication A.
186 Kröner 2016). In addition, we selected two ca. 3.45 Ga ultramafic rocks from the Dwalile Greenstone
187 Remnant (Kröner and Tegtmeyer 1994) and one 3.24 Ga trondhjemitic gneiss which intruded into the
188 grey gneisses structurally below the Dwalile Greenstone Remnant (age: personal communication A.
189 Kröner 2017). The latter sample contains inherited zircon grains of 3.49 Ga and ca. 3.64 Ga (ages:
190 personal communication A. Kröner 2017).

191 Rock types of the oldest supracrustal sequences of the BGB include one meta-tholeiite of the
192 Sandspruit Formation (KS-BA 189; supplementary material S1) and two samples of the Theespruit
193 Formation (meta-tholeiite BA 156, supplementary material S1; felsic metavolcanic rock AGC 372,
194 Kröner et al. 2013) as well as one meta-tholeiite of the Komati Formation (ZA-32a, supplementary
195 material S1). These samples span a narrower age range than the AGC granitoids from ca. 3.55 Ga to

196 3.48 Ga and are representative of the lower Onverwacht Group. In addition, $\mu^{142}Nd$ analyses were
197 conducted on a 3.46 Ga tonalite component of the Theespruit Pluton, containing heterogeneous Hf-in-
198 zircon isotopic compositions (e.g. sample BA 115 from Kröner et al. 2016 that was taken at the same
199 locality), and a 3.51 Ga sample of the Steynsdorp Pluton. More detailed descriptions are provided in
200 Kröner & Tegtmeyer (1994), Kröner et al. (2013, 2014, 2016), and Hoffmann et al. (2016). Sample
201 localities are shown in Figure 1.
202
203 3.2 Analytical methods
204
205 The chemical separation for Nd isotopes is described in detail in the supplementary material
206 S2. Neodymium isotope measurements were performed using a Thermo-Scientific™ Triton multi-
207 collector thermal ionization mass spectrometer (MC-TIMS) at the Laboratoire Magmas et Volcans
208 (LMV), University Clermont Auvergne, Clermont Ferrand, France. Neodymium fractions were
209 dissolved in 2 µl of 2.5 N HCl and loaded onto outgassed zone-refined Re filaments. Neodymium was
210 measured as Nd^+ using a second bare Re filament as ionization filament. Each measurement was
211 performed in 27 blocks of 20 cycles each (~8 s integration) in dynamic mode using amplifier rotation.
212 The background was measured before each block. After a series of 9 blocks, readjustment of the focus
213 and a peak center were conducted. For the dynamic mode, one line of measurements was performed
214 with the mass ^{145}Nd in the central faraday cup with ^{140}Ce being monitored in the L4 and ^{147}Sm in the
215 H2 faraday cup. The second line was measured with the mass ^{143}Nd in the central faraday cup,
216 monitoring ^{138}Ba in the L4 faraday cup to check if the ionization of Nd isotopes was not hampered due
217 to a high Ba signal. If possible, samples were run repeatedly up to three times on the same filament,
218 depending on the Nd content (notation #R1, #R2, and #R3 in Table 1, respectively).
219 Roth et al. (2014b) showed that rapid sample fractionation between the sequential
220 measurement of $^{146}Nd/^{144}Nd$ and $^{142}Nd/^{144}Nd$ (2 lines acquisition) can induce large biases on dynamic
221 $^{142}Nd/^{144}Nd$ ratios. The fractionation rates calculated for samples and standards during this study are
222 on average 0.215 $ppm.s^{-1}$ and 0.175 $ppm.s^{-1}$, respectively. These values are far below the threshold

223 limit of 0.4 ppm.s^{-1}. A fractionation rate that would produce a bias on dynamic $^{142}Nd/^{144}Nd$ ratios must
224 be higher than 5 ppm.

225 Neodymium isotope ratios were corrected for mass fractionation using the exponential law and
226 $^{146}Nd/^{144}Nd = 0.7219$. Data are reported relative to the JNdi-1 standard which was measured along
227 with the samples, resulting in an average long-term $^{142}Nd/^{144}Nd$ ratio of 1.141839 ± 4.4 ppm (2s.d., n =
228 13) for the first analytical session (LMV Triton) and 1.141827 ± 4.3 ppm (2s.d., n = 17) for the second
229 session (LMV Triton Plus), if the analyses would follow a normal distribution. However, given a
230 relatively limited number of JNdi-1 analyses within the two analytical sessions, i.e. 13 and 17 times, a
231 student´s t distribution for calculating the 95% confidence interval would be more appropriate. With
232 this calculation, the deviations from the mean $^{142}Nd/^{144}Nd$ ratio for the first and second standard
233 analytical sessions result in ± 1.33 ppm and ± 1.10 ppm, respectively.

234 Available major and trace element as well as ^{147}Sm-^{143}Nd and ^{176}Lu-^{176}Hf isotope data for all
235 samples are summarized in Table S1 of the supplementary material. A summary of the analytical
236 methods for samples AGC 222, AGC 350, AGC 445, AGC 473, BA 132, BA 156, KS-BA 189, and
237 ZA-32a is provided in the supplementary material S3.

238

239

240 **4. Results**

241

242 Table 1 summarizes the results for $^{142}Nd/^{144}Nd$, $^{143}Nd/^{144}Nd$, $^{145}Nd/^{144}Nd$, $^{146}Nd/^{144}Nd$,
243 $^{148}Nd/^{144}Nd$, and $^{150}Nd/^{144}Nd$ measurements on seventeen samples from the BGB and AGC,
244 respectively. The Hawaiian basalt BHVO-2 was measured as reference material, and the data as well
245 as repeated analyses of the terrestrial standard JNdi-1 are listed in Table 1. Measurements have been
246 performed during two different analytical sessions and using the two LMV thermal ionization mass
247 spectrometers: Triton™ (session 1) and Triton Plus™ (session 2). The BHVO-2 standard yielded a
248 $\mu^{142}Nd$ of 2.4 ± 4.4 ppm, overlapping within error with the JNdi-1 terrestrial standard measured in
249 session 1. The analytical uncertainties on $^{142}Nd/^{144}Nd$ for single internal sample runs were usually
250 better than 3.9 ppm, except for two samples (AGC 350, KS-BA 189), which had internal

reproducibilities between ± 4.0 ppm and ± 5.0 ppm (Table 1). However, in the figures we report the 2s.d. external reproducibility from the standard sessions for samples that were only measured once. For repeated measurements (n = 2-3) a mean value was calculated and is also reported together with the 2s.d. of the standard sessions, because the external reproducibility of the standard is better constrained than those of the sample analyses.

Measured μ^{142}Nd values in samples of the Kaapvaal Craton range from -7.9 ± 4.4 ppm to +3.0 ± 4.3 ppm (Fig. 2). Confidently resolvable μ^{142}Nd anomalies were found in a 3.44 Ga Ngwane Gneiss (AGC 352) and two ca. 3.45 Ga (ultra-)mafic rocks from the Dwalile Supracrustal Suite (AGC 45 and 50), having μ^{142}Nd values of -7.9 ± 4.4 ppm ,-6.2 ± 4.3 ppm, and -6.1 ± 4.3 ppm, respectively.

5. Discussion

5.1 Evaluation of metamorphic disturbance

All samples from the AGC and BGB underwent metamorphic overprint up to amphibolite-facies conditions. Such metamorphic events could cause element migration and, hence, disturbance of the Nd isotope compositions by metamorphic fluids. However, our samples do not show any correlation of their μ^{142}Nd signatures with, for example, enrichment in light rare earth or large ion lithophile elements (Figure S4 of the supplementary material). Consequently, we consider the μ^{142}Nd anomalies in the AGC and BGB rocks as reflecting original source compositions.

5.2 Significance of negative ^{142}Nd signatures in Archean rocks of the Ancient Gneiss Complex

The first μ^{142}Nd data reported for the AGC provide evidence for the preservation of a negative μ^{142}Nd isotope signature throughout different lithological units of the AGC (Fig. 2). However, only three samples can be readily distinguished in terms of μ^{142}Nd compared to the modern terrestrial reference material. Nevertheless, as shown in Figure 3a, all of our analyzed samples from the BGB and AGC taken together as one population show a statistically significant offset from the standard towards negative μ^{142}Nd values. Furthermore, as illustrated in Figure 3b, a bimodal distribution can be

observed with one population of ten samples having generally negative μ^{142}Nd anomalies with an average of -5.3 ± 1.0 ppm (95% conf. int.) relative to the terrestrial standard and another population of seven samples showing no deviation from the JNdi-1 terrestrial standard with a mean μ^{142}Nd of 0.4 ± 1.2 ppm (95% conf.int.). The presence of negative μ^{142}Nd values requires the involvement of an older crustal or enriched mantle reservoir in their petrogenesis. This could have occurred either by direct melting of a Hadean enriched protocrust that remained unaffected by melting or crustal recycling since its differentiation (e.g., O'Neil et al. 2008; O'Neil and Carlson 2017) or by inheritance of a Hadean μ^{142}Nd signature from older granitoids that formed after the extinction of ^{146}Sm and were contaminated by Hadean crustal material, ultimately resulting from Hadean mantle-derived mafic melts. Alternatively, the negative μ^{142}Nd anomalies were inherited from the mantle source that underwent a differentiation event in the Hadean accompanied by a decrease of Sm/Nd and may have interacted with the early cratonic nuclei to produce granitoids with variably negative μ^{142}Nd values.

Preserved Archean continental crust is interpreted to consist, to large degrees, of juvenile TTGs, which represent direct melts of metamorphosed mafic crust (e.g., Moyen and Martin 2012 and refs. therein). However, many Archean crustal terranes are now composites of grey gneisses that have diverse origins and complex formation histories involving crustal reworking processes (e.g., Moyen 2011; Hoffmann et al. 2011). Here, interaction of mantle-derived magmas with older felsic crust may have been common, leading to further differentiation and diversification of the Archean crust and, ultimately, to stabilization of the crust (e.g., Laurent et al. 2014; Hoffmann et al. 2016). This is the case for the early Archean crust of the eastern Kaapvaal craton where, on the basis of heterogeneous Hf isotope signatures of zircons from grey gneiss samples, different studies argued for interaction of juvenile mantle-derived magmas with older felsic crust (Zeh et al. 2011; Kröner et al. 2014; Hoffmann et al. 2016) or melting of older felsic crust in the presence of zircon (e.g., Tang et al. 2014). Moreover, rare inherited Eoarchean zircon grains were found in rocks of the AGC (e.g., Kröner and Tegtmeyer 1994), thus providing additional support for the involvement of older crustal rocks in the genesis of the exposed crust. Interestingly, depleted mantle Lu-Hf model ages for zircons from the Ngwane gneisses were calculated to be up to 4.1 Ga (e.g., Zeh et al. 2011; Kröner et al. 2014). However, the complex intra-crustal differentiation processes make one-stage model ages unlikely, and the calculated

ages would only provide minimum ages for the initial extraction of melt from a hypothetical depleted mantle reservoir.

Juvenile crustal additions to the AGC were largely restricted to the mid-Paleoarchean (e.g., Zeh et al. 2011; Kröner et al. 2014; Hoffmann et al. 2016). The granitoids measured here for their $^{142}Nd/^{144}Nd$ isotope compositions cover an age range from ca. 3.66 to ca. 3.22 Ga. The only clearly resolvable negative ^{142}Nd anomaly was found in a 3.44 Ga Ngwane grey gneiss from the Mankanyane region. In this sample, the zircon Hf isotope compositions were heterogeneous (Hoffmann et al. 2016), in support of the conclusions of Kröner et al. (2014) and Hoffmann et al. (2016) that these rocks formed by melting of older crustal material. The negative $\mu^{142}Nd$ value, however not resolvable from the terrestrial standard, in the youngest 3216 Ma grey gneiss investigated in this study indicates that back-mixing of crustal components into the mantle or, alternatively, mantle reservoirs carrying the ^{142}Nd anomaly lasted at least until 3.2 Ga, and this process can potentially be traced in various granitoids of different ages.

Except for two samples of the Dwalile Greenstone Remnant (AGC 45, 50) that bear resolvable negative $\mu^{142}Nd$ anomalies, two other Palaeoarchean amphibolites (AGC 222; AGC 350) from Kubuta in central Swaziland and the Mtimane River NE of Mankayane do not show any discernable offset from the modern terrestrial $\mu^{142}Nd$ value (Fig. 2). These two amphibolites without anomalies may constitute end members during complex crustal assimilation and mixing processes, involving melts derived from older Ngwane gneiss basement as suggested by Hoffmann et al. (2016) for the 3.48-3.43 Ga Tsawela gneiss suite. Hence, the most negative $\mu^{142}Nd$ values in the Ngwane and Tsawela gneisses may still represent intermediate values, providing that the two modern-like amphibolites measured in this study are indeed representatives of juvenile mafic melts. Unfortunately, these two amphibolites are infolded in the Ngwane gneiss, and intrusive relationships between the two components are not preserved at these localities.

For the Dwalile Greenstone Remnant, Kröner and Tegtmeyer (1994) reported initial $\varepsilon^{143}Nd$ data for amphibolites, hornblende-schists, and metasediments ranging from positive to negative $\varepsilon^{143}Nd_{(t)}$ values that are in agreement with variable degrees of crustal contamination as well as incorporation of older crustal detritus in sedimentary rocks of the belt. Moreover, inherited zircon

grains, up to 3.7 Ga in age, were reported in the gneissic basement structurally below the Dwalile Geenstone Remnant (Kröner and Tegtmeyer 1994), indicating an older felsic crustal basement. So far, there are no detailed studies on the geochemical composition of the AGC mafic rocks, but crustal contamination of our two amphibolite samples from Dwalile can at least be excluded, on the basis of flat trace element patterns and depleted to chondritic Hf-Nd isotopic compositions. The observed negative μ^{142}Nd anomalies of Dwalile samples AGC 45 and AGC 50 may thus be representative of the tapped mantle source. Interestingly, enriched (i.e., negative) μ^{142}Nd and μ^{182}W deviations have been reported for komatiites of the 3.55 Ga Schapenburg Greenstone remnant ca. 65 km away (Puchtel et al. 2016). These signatures were interpreted by the authors as being of mantle origin, likely related to fractionation processes involving Ca-Mg perovskite in an early magma ocean. Decoupling of ^{142}Nd and ^{143}Nd systematics with mean negative μ^{142}Nd (μ^{142}Nd = -5 ± 2.8 ppm) and positive ε^{143}Nd (ε^{143}Nd = +2.4 ± 0.1) in Schapenburg komatiites was interpreted to reflect a melt depletion event within the komatiite source at the end of the lifetime of ^{146}Sm at ca. 4027 Ma. Hence, both the mafic precursor rocks of AGC crust and the mantle-derived rocks in the Schapenburg area may have tapped the same mantle reservoirs.

5.3 Relation between the Ancient Gneiss Complex and the Barberton Greenstone Belt

The AGC is tectonically separated from the supracrustal BGB by the Phoponyane shear zone northwest of Pigg´s Peak town, possibly indicating that the two terranes were originally separated and amalgamated at around 3.3 to 3.2 Gyr (De Ronde and De Wit, 1994) or 3.55 to 3.42 Gyr ago (Kröner et al., 1996), respectively. In contrast to the AGC, the majority of rock units of the BGB terrane, namely the 3.55 Ga to 3.53 Ga amphibolites of the lowermost Onverwacht Group as well as the 3.51 Ga Steynsdorp and 3.46 Ga Theespruit plutons, do not show any deviation in μ^{142}Nd from the terrestrial standard (Fig. 2). Hence, these units have not inherited a Hadean crustal or mantle reservoir that differentiated during the lifetime of ^{146}Sm. However, two samples of the lower Onverwacht Group, a 3.55 Ga felsic volcanic rock (AGC 372; Theespuit Fm.) and a 3.48 Ga meta-tholeiite (ZA-32a; Komati Fm.) show a tendency towards negative μ^{142}Nd anomalies (Fig. 2) that are not fully

resolvable from the JNdi-1 terrestrial standard. Yet, we consider these features as being important for the interpretation of the geodynamic setting in which the BGB formed.

Kröner et al. (2013, 2016) proposed that the felsic metavolcanic rocks of the lower Onverwacht Group originated from interaction of an older crustal source with juvenile, underplated material. These authors based their conclusions on heterogeneous Hf isotope compositions in zircons and calculated crustal model ages for the precursor ranging from 3.60 to 3.95 Ga. However, the negative μ^{142}Nd signature (μ^{142}Nd = -5.6 ± 4.4 ppm) of the felsic volcanic rock (AGC 372) investigated in this study is not very pronounced, and it is likely that the ca. 3.60 to 3.95 Ga precursors only carried a diluted Hadean isotope signature because they formed after the lifetime of ^{146}Sm. Such a model would be in agreement with the contribution of AGC-like basement beneath the lower Onverwacht Group as a source for felsic volcanism within the BGB. This hypothesis is also supported by ca. 3.7 Ga inherited zircon grains reported from Theespruit felsic volcanic rocks (Roerdink et al. 2016) and from the adjacent 3.2 Ga Vlakplaats pluton (Kröner et al. 1996). Therefore, it is likely that felsic volcanic rocks of the BGB were initially fed by magma chambers that are elsewhere represented by second generation granitoids such as the Tsawela gneiss suite that carry a diluted Hadean μ^{142}Nd signature, as they are exposed at crustal levels of the AGC (Hoffmann et al. 2016).

Another interesting observation of this study is the tendency towards negative μ^{142}Nd in the younger meta-tholeiite sample of the ca. 3.48 Ga Komati Formation (sample ZA 32a) with a μ^{142}Nd value of -5.4 ± 4.3 ppm (Fig. 2). Previous studies focused exclusively on komatiites from the Barberton type locality and from the 3.26 Ga Weltevreden Fm. that do not preserve any resolvable μ^{142}Nd deviation (Caro et al. 2006; Puchtel et al. 2016). Yet, initial ε^{176}Hf and initial ε^{143}Nd compositions for rocks from the Komati Fm. are predominantly positive, showing no evidence of contamination by older crust (Blichert-Toft and Arndt 1999; Blichert-Toft et al. 2015). In contrast, trace element compositions of some spinifex-textured komatiites of the Komati Fm. were interpreted to reflect contamination with older continental crust (Robin-Popieul et al. 2012). The flat trace element pattern as well as the juvenile Hf-Nd isotope signature of meta-tholeiite ZA 32a (supplementary material S1) are not in agreement with crustal contamination. Hence, two different mantle reservoirs may have been tapped by Komati Fm. magmas producing komatiites with modern-like μ^{142}Nd on the

391 one side and tholeiites with negative μ^{142}Nd on the other side, possibly reflecting mixing between
392 ascending mantle plume magmas and ambient upper mantle or lithospheric mantle (e.g., Sossi et al.
393 2016, and references therein) that bear a small ^{142}Nd deficit.
394
395 5.4 Origin of the negative μ^{142}Nd signatures in rocks of the AGC and BGB
396
397 In Figure 3b, the samples investigated in this study plot in a bimodal distribution. One trend
398 comprises seven samples with no μ^{142}Nd anomalies and the other trend includes ten samples having a
399 tendency to negative μ^{142}Nd signatures. The trends may reflect two separate mantle reservoirs.
400 Interestingly, both reservoirs must have been tapped concurrently, independent of magmatic age and
401 lithological unit. Collectively, both μ^{142}Nd reservoirs are represented by samples spanning an age
402 range from 3.66 Ga to 3.23 Ga (for the μ^{142}Nd = +0.4 reservoir) and 3.55 Ga to 3.22 Ga (for the
403 negative μ^{142}Nd reservoir). Notably, both reservoirs are represented by samples of the AGC and BGB.
404 The enriched end member, as represented by the Dwalile amphibolites, was therefore mantle-
405 derived and interacted with differentiated AGC crust. Since some (ultra-)mafic Dwalile rocks were
406 potentially crustally contaminated (e.g., Kröner and Tegtmeyer 1994) the measured value may thus not
407 represent the true negative μ^{142}Nd value of the enriched reservoir, provided that the contaminating
408 crust had positive or modern-like μ^{142}Nd. The original values for this reservoir may be represented by
409 the mantle source tapped by the 3.55 Ga Schapenburg komatiites, which yielded negative μ^{142}Nd
410 values as low as -13.4 ppm compared to the terrestrial standard (Puchtel et al. 2016; Fig. 3c). This may
411 indicate that the negative μ^{142}Nd values of the Komati Fm. tholeiite and the Dwalile amphibolites as
412 well as some granitoids may represent intermediate values which already reflect mixing between
413 enriched and modern-like mantle reservoir end members. However, it is difficult to estimate the exact
414 mixing parameters and whether the two reservoirs were genetically related to each other.
415 For mantle derived rocks, the combined use of ^{142}Nd and ^{143}Nd isotope systematics can be
416 applied as a tool for the calculation of model ages reflecting Hadean mantle differentiation events
417 (e.g., Harper and Jacobsen 1992; Caro et al. 2006; Rizo et al. 2011). However, for granitoids with
418 complex histories such as those of the AGC, this method is not applicable due to multiple

metamorphic resetting and mixing of the ^{147}Sm-^{143}Nd system during crustal reworking, which occurred after extinction of the ^{146}Sm-^{142}Nd system, leading to decoupling of the two systems.

As the (ultra-)mafic samples from Dwalile and the tholeiite from Barberton seem to be derived from an enriched reservoir, it is likely that their mantle source already carried an enriched ^{142}Nd signature. Assuming that the (ultra-)mafic Dwalile rocks and the Komati Fm. tholeiite represent mantle source compositions, and provided that metamorphism did not disturb their $^{147}Sm/^{144}Nd$, a minimum age for the differentiation of their mantle sources can be calculated (Figure 4). As shown in Figure 4, the mantle source from which the Dwalile komatiites and the Komati tholeiite were derived may have differentiated at 4.3 Gyr ago.

The ultimate origin of the negative $\mu^{142}Nd$ anomaly in the Dwalile komatiites and the Komati tholeiite may therefore be related to early magma ocean differentiation (e.g., Puchtel et al. 2016) or to recycling of enriched Hadean protocrust back into the mantle (Guitreau et al. 2012; Caro et al. 2017). However, it is not possible to confidently constrain which of these two possibilities is applicable to the AGC and BGB (ultra-)mafic rocks.

Constraining the origin of the enriched ^{142}Nd signature in the AGC granitoids is similarly challenging. A direct contribution of enriched mafic Hadean protocrust to the TTG precursors of the AGC, sporadically occurring over a time period of ca. 1 billion years, is likely. Such a process has recently been suggested for the Hudson Bay terrane by O'Neil and Carlson (2017). Alternatively, the negative $\mu^{142}Nd$ anomalies in the granitoids could also be the result of repeated re-melting of granitoid crust that inherits a negative $\mu^{142}Nd$ signature, ultimately derived from recycled enriched Hadean protocrust, and mixing with mafic melts that formed after the extinction of ^{146}Sm. This hypothesis is based on the fact that the Nd budget would be dominated by the crustal rocks during crustal reworking. For example, the Dwalile mafic and ultramafic rocks have Nd contents of 5.56 and 8.19 ppm, respectively, whereas the Nd concentrations of the granitoids carrying the negative ^{142}Nd signature range from 12.2 to 37.5 ppm (Table S1).Decoupling of enriched ^{142}Nd isotope signatures in the AGC granitoids from the Hf isotope record as represented by zircons (Zeh et al. 2011; Kröner et al. 2014; Hoffmann et al. 2016), where a trend toward more radiogenic compositions with time can be observed (Hoffmann and Kröner in press), would argue for the latter hypothesis. This decoupling is

447 independent of age or sample locality and confirms that both the enriched and modern-like reservoirs
448 contributed to the formation of AGC rocks since at least the early Archean.

449 In summary, our study reveals that two mantle reservoirs were involved in the formation of the
450 AGC and BGB rocks in the eastern Kaapvaal Craton that can be distinguished by means of their
451 μ^{142}Nd signatures. The enriched ^{142}Nd reservoir likely has a minimum mantle differentiation age of 4.3
452 Ga (Fig. 4) and was incorporated into the (ultra-)mafic Dwalile and some Komati Fm. rocks since
453 some 3.45 Gyr ago. In contrast, the modern-like reservoir is trapped in mafic AGC and BGB rocks
454 ranging in age from 3.55 to ca. 3.40 Ga. It would appear that no mixing occurred between the two
455 reservoirs throughout the Archean or that such mixing cannot be resolved within the analytical error.
456
457 5.5 Worldwide sources of early enriched and depleted ^{142}Nd signatures through time
458
459 Decreasing negative and positive Hadean μ^{142}Nd anomalies through time (Figure 5a,b) have
460 been interpreted to represent increasing homogenization of early differentiated reservoirs (e.g., Boyet
461 and Carlson 2005; Caro et al. 2006; Bennett et al. 2007; Rizo et al. 2012). However, it is ambiguous as
462 to whether this homogenization of early-differentiated reservoirs is only seen in mantle-derived rocks
463 through time or also in the stabilized cratons. Figure 5a shows all published μ^{142}Nd data for rocks
464 directly derived from mantle melts, and Figure 5b depicts μ^{142}Nd data for felsic crustal rocks with ages
465 of ca. 4.3 to ca. 2.65 Ga. The compilation in Figure 5a indicates that enriched and depleted ^{142}Nd
466 mantle reservoirs were only partially homogenized by 2.65 Ga and that enriched and depleted sources
467 were, in fact, tapped by mantle-derived rocks throughout the Archean. Felsic crustal rocks, however,
468 can preserve the anomaly over longer time scales than mafic-ultramafic rocks since they are reworked
469 from older rocks that share enriched or depleted ^{142}Nd signatures ultimately derived from stabilized
470 mafic precursors (e.g., Roth et al. 2014a; O'Neil and Carlson 2017). Alternatively, the signatures in
471 felsic rocks may indicate protocrustal material that was recycled back into the mantle (Guitreau et al.
472 2012; Caro et al. 2017). In the former case, enriched or depleted ^{142}Nd signatures are tapped directly
473 from a Hadean protocrust, whereas in the latter case the ^{142}Nd anomalies are traced by basaltic crust
474 that was formed by re-enriched mantle material. Our study on the eastern Kaapvaal Craton reveals that

475 ancient enriched mantle reservoirs were likely present until at least 3.45 Ga, as represented by the
476 Dwalile amphibolites, thus confirming earlier studies from Greenland (Rizo et al. 2012) and
477 Schapenburg (Puchtel et al. 2016), as well as Acasta where the most negative μ^{142}Nd values are found
478 in samples with low SiO_2 (Roth et al. 2014a). Further melting of such mafic material, as well as of
479 older felsic crust, incorporated negative μ^{142}Nd signatures in crustal rocks of the AGC until at least
480 3.22 Ga. This indicates that re-mixing of components containing inherited enriched ^{142}Nd crustal or
481 mantle reservoirs in the eastern Kaapvaal Craton lasted for more than 1 Gyr from the initial
482 differentiation events in the Hadean at ca. 4.3 Ga to the Mesoarchean at about 3.2 Ga.

483 Our study reveals that crustal nuclei may have tapped two completely separate mantle sources
484 that were present throughout most of the Archean. Mixing between the two sources may have taken
485 place, but is not reflected in our dataset (Fig. 5a,b). Nevertheless, the large range in complementary
486 enriched and depleted ^{142}Nd isotope signatures in other Archean cratons such as in Canada or
487 Greenland (Fig. 5a) possibly reflects multiple mantle reservoirs that may have mixed with each other
488 instead of preserving single-stage processes, i.e., direct tapping of Hadean crustal or mantle material.

489

490 **6. Conclusions**

491

492 We report the first high-precision ^{142}Nd/^{144}Nd analyses for well characterized granitoids and
493 meta-tholeiites (amphibolites) of the Ancient Gneiss Complex (Swaziland) and the lower Onverwacht
494 Group of the Barberton Greenstone Belt (South Africa). Our study reveals that representative well-
495 preserved crustal and mantle-derived rocks of the AGC and BGB show variable μ^{142}Nd values ranging
496 from -7.9 ± 4.4 ppm to +3.0 ± 4.3 ppm. As reflected by their ^{142}Nd/^{144}Nd isotope compositions, two
497 different mantle reservoirs must have been involved in crust-forming processes between 3.66 and 3.22
498 Ga. The metamorphic rocks sampling the two reservoirs are indistinguishable in terms of age,
499 lithology or sample locality. Negative μ^{142}Nd anomalies indicate the involvement of an early-enriched
500 mantle reservoir in the formation of the AGC that differentiated in the Hadean during the lifetime of
501 ^{146}Sm. This reservoir is likely entirely mantle-derived and was possibly reworked throughout the
502 Archean, yielding a ^{142}Nd/^{144}Nd model age of ca. 4.3 Ga. The presence of negative μ^{142}Nd anomalies

in mantle-derived rocks as late as 3.45 Ga confirms the presence of enriched ^{142}Nd reservoirs in the Paleoarchean mantle. Reworking of crustal rocks may have transferred the enriched signature to granitoids of the AGC that are as young as 3.22 Ga. Parallel to AGC crust that was derived from enriched mantle domains, other mantle-derived rocks and complementary granitoids of the AGC and the BGB were derived from mantle domains that do not show evidence for early differentiation events during the lifetime of ^{146}Sm. Our finding of enriched and modern-like mantle reservoirs by means of ^{142}Nd in the Kaapvaal Craton raises the question of whether other Archean cratons such as in West Greenland, Canada or Western Australia underwent a similar complex reservoir mixing history instead of single-stage processes. Such parallel behavior of enriched and depleted mantle and crustal domains may have played a more pronounced role in the formation of Archean cratons around the world than previously thought.

Acknowledgements

JEH and KS thank the Deutsche Forschungsgemeinschaft (DFG) for financial support through grants HO4697/1-1 and HO4697/1-2. AK acknowledges DFG grant KR590/92-1. CM acknowledges funding by DFG grants Mu 1406/8 and Mu 1406/18. MB thanks the Excellence initiative N° ANR-10-LABX-0006, the Région Auvergne, the European Regional Development. We thank Tsuyoshi Iizuka and a second anonymous reviewer for their constructive and helpful comments that improved our manuscript. We thank Monika Feth for laboratory support and Alexander Balduin for help with sample preparation and the geological map. KS thanks the LMV in Clérmont-Ferrand for hospitality during her visit for analytical work. This is a contribution to the SPP1833 Project '*Building a habitable Earth*' funded by the DFG. This project has received funding from the European Union´s Horizon 2020 research and innovation program under Grant Agreement N° 682778.

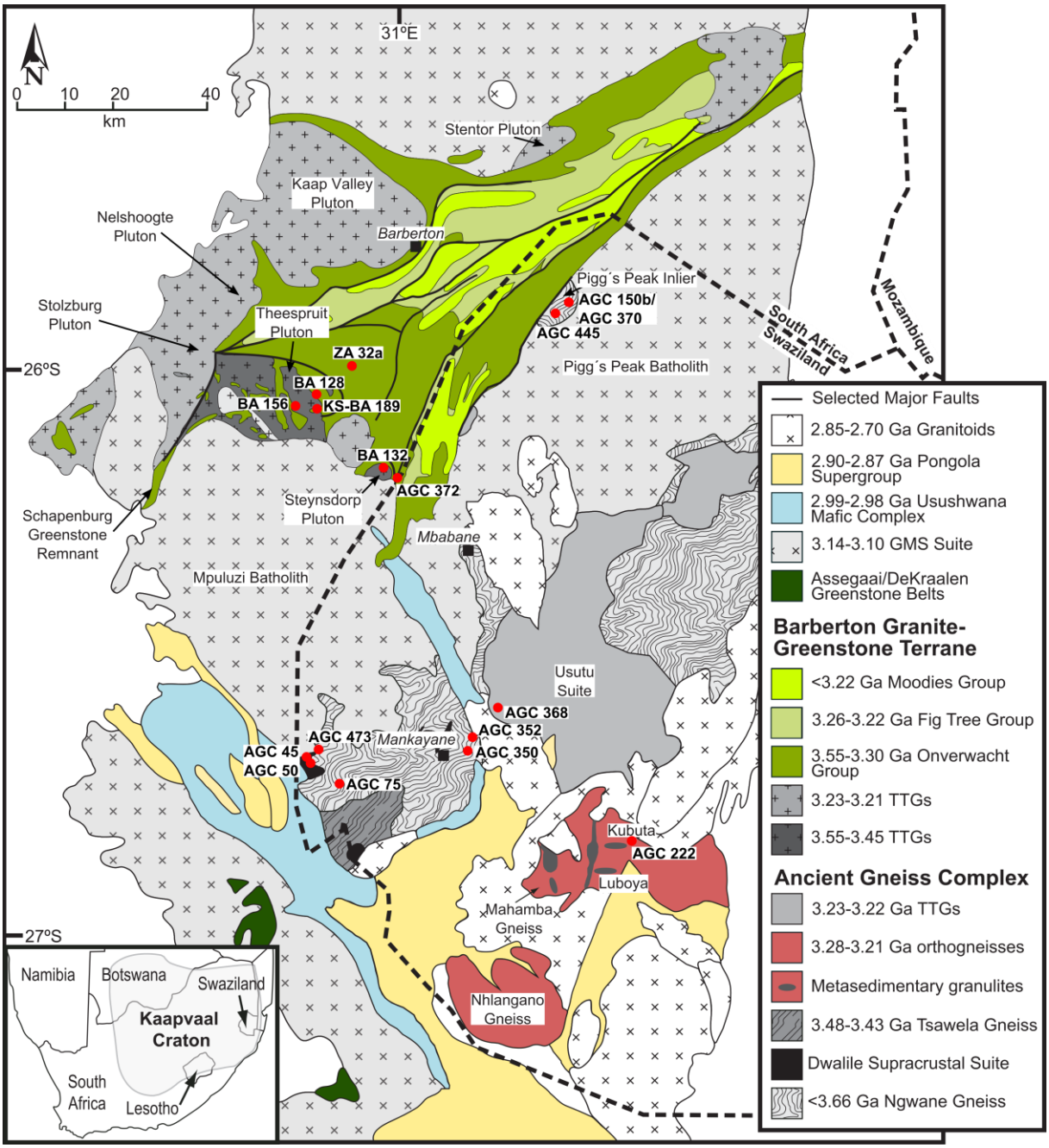

Figure 1: Simplified geological map of the Ancient Gneiss Complex (Swaziland) and Barberton Greenstone Belt (South Africa) in the eastern Kaapvaal Craton. Red dots mark sample localities of the investigated felsic, mafic, and ultramafic rocks. Map modified after Van Schijndel et al. (2017).

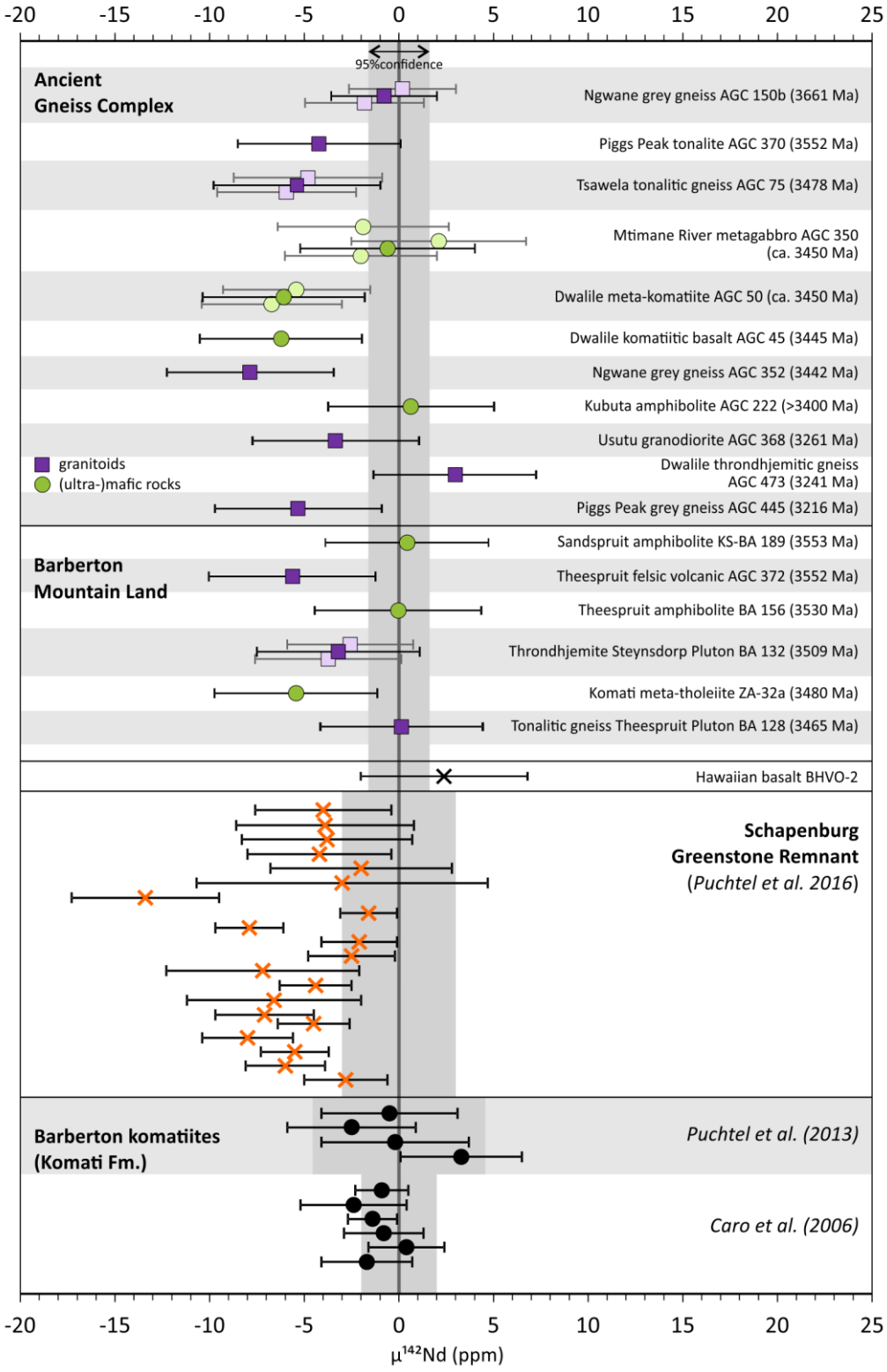

533

534 Figure 2: Measured $\mu^{142}Nd$ values for the studied AGC and BGB rocks. Usually single measurements
535 of granitoids (purple) and (ultra-)mafic rocks (green) are reported except for samples AGC 150b, AGC
536 75, AGC 350, AGC 50, BA 132, and BA 128 where single measurements are represented by lighter
537 symbols and the mean values are represented by the dark filled symbols. Samples AGC 352, AGC 45,

and AGC 50 show resolvable negative anomalies relative to the terrestrial value (grey vertical box). Additionally, four samples (AGC 75, 372, 445, and ZA-23a) show a tendency to slightly negative μ^{142}Nd values that are, however, within error not unambiguously resolvable from the JNdi-1 terrestrial standard. The 95% confidence interval of the JNdi-1 standard was ± 1.3 ppm for the first analytical session and ± 1.1 ppm for the second analytical session (grey vertical box). Literature data for Barberton and Schapenburg komatiites is shown for comparison.

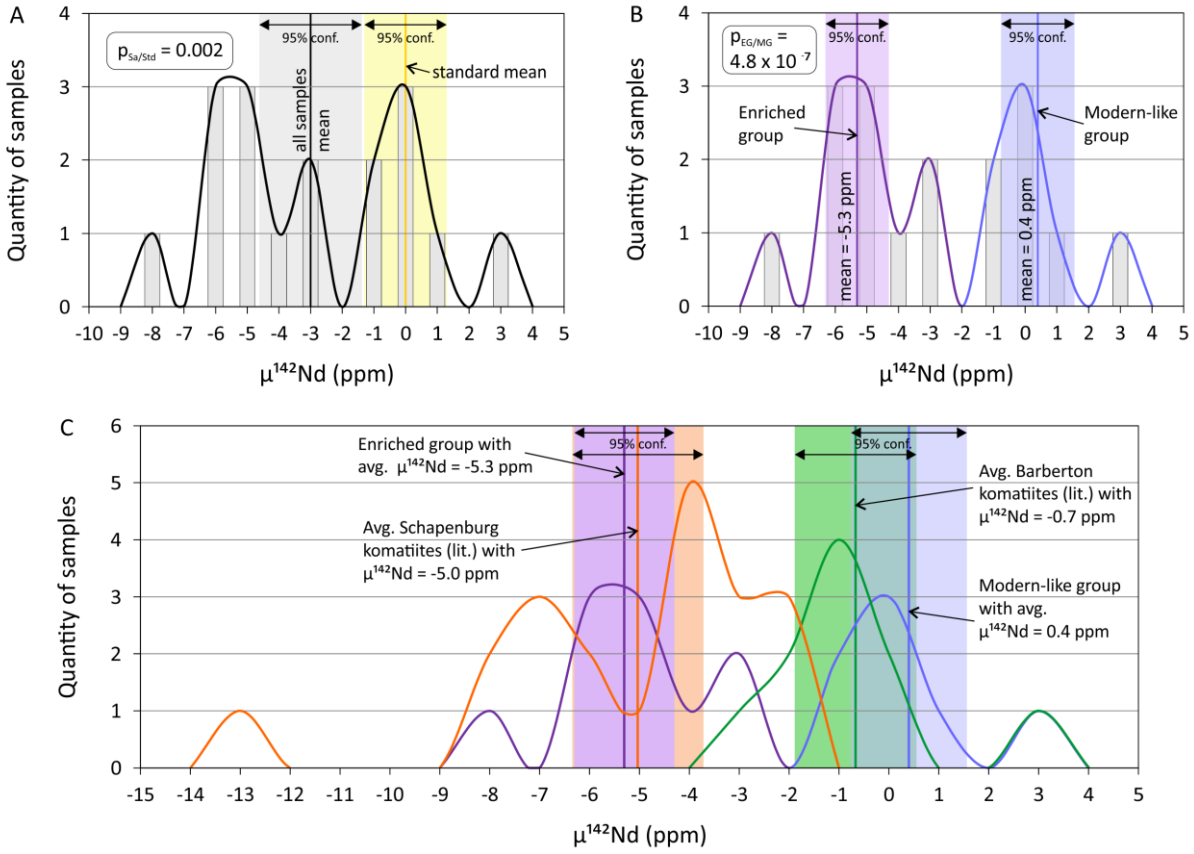

Figure 3: Histograms of μ^{142}Nd data. A) Distribution of analyzed samples (black line with grey bars) with an average μ^{142}Nd of -3.0 ± 1.6 ppm (95% conf.int.). Additionally, the average μ^{142}Nd of 0 ± 1.3 ppm (95% conf.int.) of the standard analyses is also shown (yellow line and yellow shaded area). A student´s t-test of the two populations resulted in a probability $p_{Sa/St}$ of 0.002 (i.e. 0.2 %) that the two populations belong to one group, i.e. the two groups are statistically significantly different. B) Distribution of analyzed samples divided into a bimodal distribution with an enriched group having an average μ^{142}Nd of -5.3 ± 1.0 ppm (95% conf.int., n = 10; purple line and shaded area) and a modern-like group averaging +0.4 ± 1.2 ppm (95% conf.int., n = 7; blue line and shaded area). A student´s t-

554 test of the two groups resulted in a probability $p_{EG/MG}$ of $4.8x10^{-7}$ (i.e. 0.000048 %) that the two
555 populations belong to one group, i.e. the two groups are statistically significantly different. C)
556 Comparison of our data to literature data of the Schapenburg komatiites (orange line and shaded area;
557 Puchtel et al. 2016) and Barberton komatiites (green line and shaded area; Caro et al. 2006, Puchtel et
558 al. 2013). The Schapenburg komatiites have an average $\mu^{142}Nd$ of -5.0 ± 1.3 ppm (95% conf.int.)
559 resembling our enriched group of samples, and the Barberton komatiites have an average $\mu^{142}Nd$ of -
560 0.7 ± 1.2 ppm (95% conf.int.) resembling our modern-like group of samples, which confirms our
561 interpretation of the involvement of two mantle sources in the formation of these rocks.
562

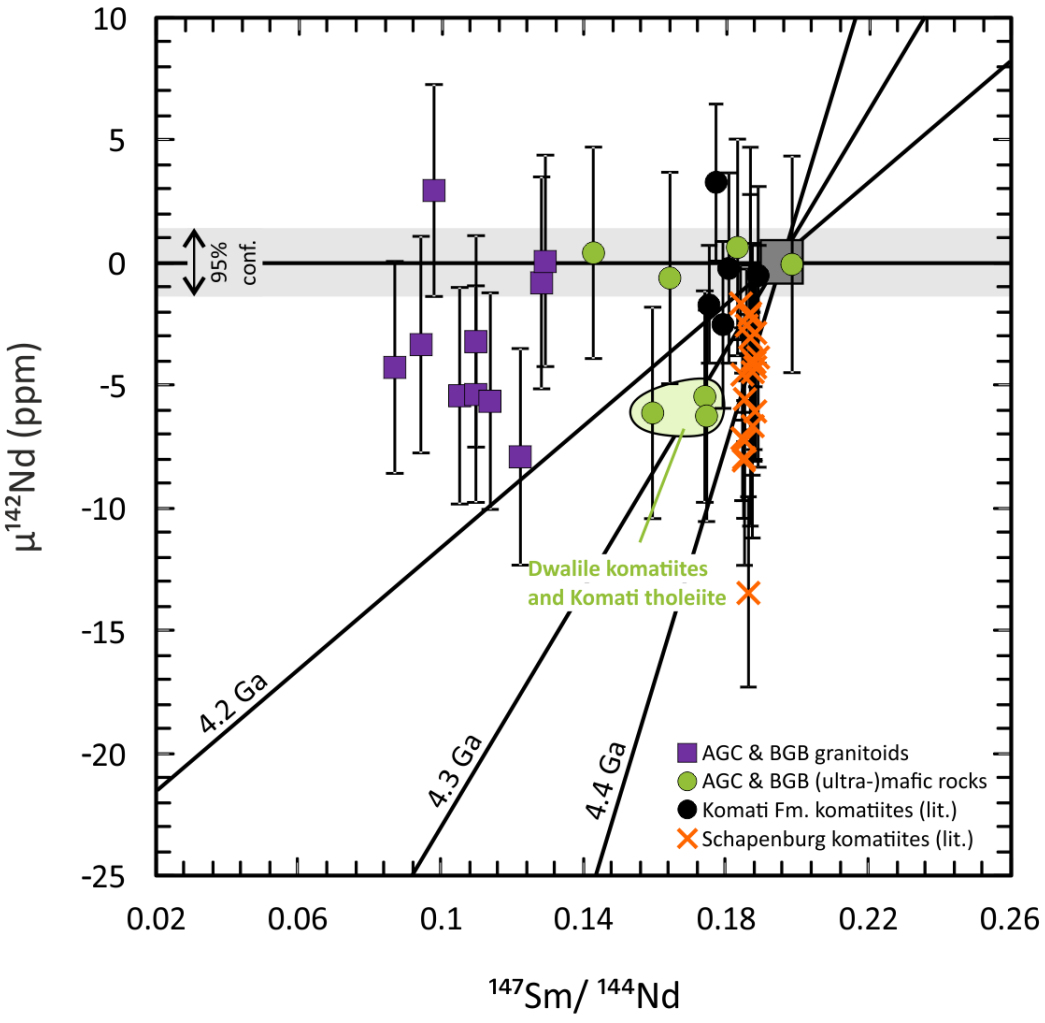

563
564 Figure 4: $\mu^{142}Nd$ vs. $^{147}Sm/^{144}Nd$. The Dwalile komatiites and Komati Fm. tholeiite analyzed in this
565 study yielded a mantle source differentiation age of ca. 4.3 Ga, provided that their $^{147}Sm/^{144}Nd$ ratio
566 was not disturbed by secondary alteration. However, given the sample uncertainties, the source

differentiation age could vary between 4.1 and 4.4 Ga. The granitoids showing negative μ^{142}Nd signatures inherited a contribution from the enriched mantle reservoir. Another group of granitoids and mafic rocks of the AGC and BGB did not tap the enriched mantle reservoir. The dark grey square represents the chondritic Sm/Nd ratio of 0.196. The light grey box represents the 95% confidence interval of 1.3 ppm obtained for measurements of the JNdi-1 terrestrial standard. The figure is modified after O´Neil and Carlson (2017), who calculated reference isochrones for 4.4-, 4.3-, and 4.2-billion years old crustal reservoirs that were derived from a mantle with a chondritic Sm/Nd ratio. Literature data are from Caro et al. (2006), Puchtel et al. (2013, 2016).

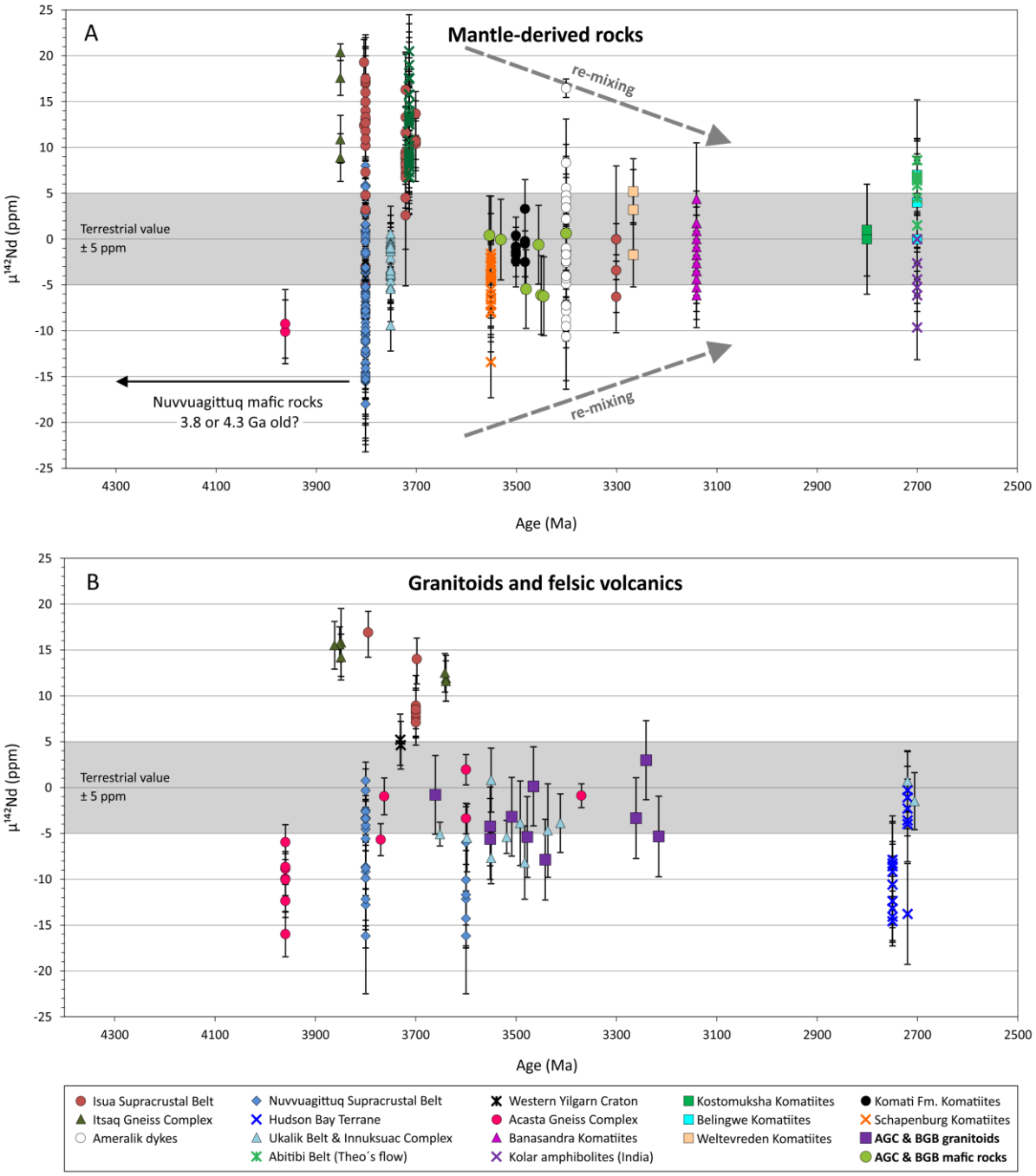

Figure 5: Compilation of published μ^{142}Nd data against age for Archean cratons worldwide, including literature and our data for the Kaapvaal Craton. A) Mantle-derived rocks against age. B) Granitoid rocks against age. The compiled μ^{142}Nd anomalies for mantle-derived rocks indicate re-mixing of reservoirs with positive and negative μ^{142}Nd signatures with time. A similar trend is overserved for the granitoids, but the mechanism may be different for different tectonic environments (see text). The age of mafic Nuvvuagittuq rocks is currently under debate. References: Boyet and Carlson 2006; Caro et al. 2006, 2017; Bennett et al. 2007; O`Neil et al. 2008, 2012, 2016; Rizo et al. 2011, 2012, 2013;

584 Debaille et al. 2013; Puchtel et al. 2013, 2016; Roth et al. 2013, 2014a; Maya et al. 2016; O´Neil and
585 Carlson 2017.
586
587
588 **References**

589 Anhaeusser, C.R., 2014. Archaean greenstone belts and associated granitic rocks – A review. J Afr.
590 Earth Sci. 100, 684-732.

591 Bennett, V.C., Brandon, A.D., Nutman, A.P., 2007. Coupled ^{142}Nd–^{143}Nd isotopic evidence for
592 Hadean mantle dynamics. Science 318, 1907–1910.

593 Blichert-Toft, J., Arndt, N.T., 1999. Hf isotope compositions of komatiites. Earth Planet. Sci. Lett.
594 171, 439-451.

595 Blichert-Toft, J., Arndt, N.T., Wilson, A. Coetzee, G., 2015. Hf and Nd isotope systematics of early
596 Archean komatiites from surface sampling and ICDP drilling in the Barberton Greenstone Belt, South
597 Africa. Am. Mineralogist 100, 2396-2411.

598 Boyet M., Albarède F., Garcia M.O., Pik R., 2005. A search for ^{142}Nd evidence of primordial mantle
599 heterogeneities in plume basalts. Geophys. Res. Lett. 32, No 32, L04306.

600 Boyet, M., Carlson, R.W., 2005. ^{142}Nd evidence for early (>4.53 Ga) global differentiation of the
601 silicate Earth. Science 309, 576-581.

602 Boyet M., Carlson R.W., 2006. A new geochemical model for the Earth's mantle inferred from
603 146Sm–142Nd systematics. Earth Planet. Sci. Lett. 250, 254-268.

604 Caro, G., Bourdon, B., Wood, B.J., Corgne, A., 2005. Trace-element fractionation in Hadean mantle
605 generated by melt segregation from a magma ocean. Nature 436 249-249.

606 Caro G., Bourdon B., Birck J.L. and Moorbath S., 2006. High-precision ^{142}Nd/^{144}Nd measurements in
607 terrestrial rocks: constraints on the early differentiation of the Earth's mantle. Geochim. Cosmochim.
608 Acta 70, 164-191.

609 Caro, G., Morino, P., Mojzsis, S.J., Cates, N.L., Bleeker, W., 2017. Sluggish Hadean geodynamics:
610 Evidence from coupled ^{146,147}Sm-^{142,143}Nd systematics in Eoarchean supracrustal rocks of the Inukjuak
611 domain (Québec). Earth Planet. Sci. Lett. 457, 23-37.

612 Corgne, A., Liebske, C., Wood, B.J., Rubie, D.C., Frost, D.J., 2005. Silicate perovskite-melt
613 partitioning of trace elements and geochemical signature of a deep perovskitic reservoir. Geochim.
614 Cosmochim. Acta 69, No. 2, 485-496.

615 Debaille, V., O´Neill, C., Brandon, A.D., Haenecour, P., Yin, Q.-Z., Mattielli, N., Treiman, A.H.,
616 2013. Stagnant-lid tectonics in early Earth revealed by ^{142}Nd variations in late Archean rocks. Earth
617 Planet. Sci. Lett. 373, 83-92.

618 De Ronde, C.E.J., De Wit, M.J., 1994. Tectonic history of the Barberton greenstone belt, South Africa:
619 490 million years of Archean crustal evolution. Tectonics 13, 983-1015.

620 Dziggel, A., Armstrong, R.A., Stevens, G., Nasdala, L., 2005. Growth of zircon and titanite during
621 metamorphism in the granitoid-gneiss terrane south of the Barberton greenstone belt, South Africa.
622 Mineral. Mag. 69, 1019-1036.

623 Guitreau, M., Blichert-Toft, J., Martin, H., Moijzsis, S.J., Albarède, F., 2012. Hafnium isotope
624 evidence from Archean granitic rocks for deep-mantle origin of continental crust. Earth Planet. Sci.
625 Lett. 337-338, 211-223.

626 Harper, C.L., Jacobsen, S.B., 1992. Evidence from coupled ^{147}Sm–^{143}Nd and ^{146}Sm–^{142}Nd systematics
627 for very early (4.5-Gyr) differentiation of the Earth's mantle, Nature 360 728-732.

628 Hoffmann, J.E., Kröner, A. Early Archean crustal evolution in southern Africa - an updated record of
629 the Ancient Gneiss Complex of Swaziland. In: Van Kranendonk, M., Bennett, V., Hoffmann, J.E.
630 (Eds.) Earth´s oldest rocks. Elsevier, 2nd edition, In press.

631 Hoffmann, J.E., Kröner, A., Hegner, E., Viehmann, S., Xie, H., Iaccheri, L.M., Schneider, K.P.,
632 Hofmann, A., Wong, J., Geng, H., Yang, J., 2016. Source composition, fractional crystallization and
633 magma mixing precesses in the 3.48-3.43 Ga Tsawela tonalite suite (Ancient Gneiss Complex,
634 Swaziland) - Implications for Palaeoarchaean geodynamics. Precambrian Res. 276, 43-66.

635 Hoffmann, J.E., Münker, C., Næraa, T., Rosing, M.T., Herwartz, D., Garbe-Schönberg, D.,
636 Svahnberg, H., 2011. Mechanisms of Archean crust formation inferred from high-precision HFSE
637 systematic in TTGs. Geochim. Cosmochim. Acta 75, 4157-4178.

638 Iizuka, T., Komiya, T., Ueno, Y., Katayama, I., Uehara, Y., Maruyama, S., Hirata, T., Johnson, S.P.,
639 Dunkley, D.J., 2007. Geology and zircon geochronology of the Acasta Gneiss Complex, northwestern
640 Canada: new constraints on its thermal history. Precambrian Res. 153, 179-208.

641 Jackson, M.P.A., 1984. Archaean structural styles in the Ancient Gneiss Complex of Swaziland, South
642 Africa. In: Kröner, A., Greiling, R. (Eds.), Precambrian Tectonics Illustrated. Stuttgart,
643 Schweizerbart'sche, Verlagsbuchhandlung, pp. 1-18.

644 Kemp, A.I.S., Wilde, S.A., Hawkesworth, C.J., Coath, C.D., Nemchin, A., Pidgeon, R.T., Vervoort,
645 J.D., DuFrane, S.A., 2010. Hadean crustal evolution revisited: New constraints from Pb-Hf isotope
646 systematics of the Jack Hills zircons. Earth Planet. Sci. Lett. 296, 45-56.

647 Kröner, A., Byerly, G.R., Lowe, D.R., 1991. Chronology of early Archean granite-greenstone
648 evolution of the Barberton Mountain Land, South Africa, based on precise dating by single zircon
649 evaporation. Earth Planet. Sci. Lett. 103(1-4), 41-54.

650 Kröner, A., Hegner, E., Wendt, J.I., Byerly, G.R., 1996. The oldest part of the Barberton granitoid-
651 greenstone terrain, South Africa: evidence for crust formation between 3.5 and 3.7 Ga. Precambrian
652 Res. 78(1-3), 105-124.

653 Kröner, A., Hoffmann, J.E., Xie, H., Münker, C, Hegner, E., Wan, Y., Hofmann, A., Liu, D., Yang, J.,
654 2014. Generation of early Archaean grey gneisses through melting of older crust in the eastern
655 Kapvaal craton, southern Africa. Precambrian Res. 255, 823-846.

656 Kröner, A., Hoffmann, J.E., Xie, H., Wu, F., Münker, C., Hegner, E., Wong, J., Wan, Y., Liu, D.,
657 2013. Generation of early Archaean felsic greenstone volcanic rocks through crustal melting in the
658 Kapvaal craton, southern Africa. Earth Planet. Sci. Lett. 381, 188-197.

659 Kröner, A., Tegtmeyer, A., 1994. Gneiss-greenstone relationships in the Ancient Gneiss Complex of
660 southwestern Swaziland, southern Africa, and implications for early crustal evolution. Precambrian
661 Res. 67, 109-139.

662 Kröner, A., Wendt, J.I., Milisenda, C., Compston, W., Maphalala, R., 1993. Zircon geochronology and
663 Nd isotope systematics of the Ancient Gneiss Complex, Swaziland, and implications for crustal
664 evolution. In: Kröner, A. (Ed.), The Ancient Gneiss Complex: Overview Papers and Guidebook for
665 Excursion. Geol. Surv. Mines Dep. Swaziland Bull. No. 11, pp. 15-37.

666 Kröner, A., Anhaeusser, C.R., Hoffmann, J.E., Wong, J., Geng, H., Hegner, E., Xie, H., Yang, J., Liu,
667 D., 2016. Chronology of the oldest supracrustal sequences in the Palaeoarchaean Barberton
668 Greenstone Belt, South Africa and Swaziland. Precambrian Res. 279, 123-143.

669 Laurent, O., Martin, H., Moyen, J.F., Doucelance, R., 2014. The diversity and evolution of late-
670 Archean granitoids: evidence for the onset of modern-style plate tectonics between 3.0 and 2.5 Ga.
671 Lithos 205, 208-235.

672 Lowe D.R., Byerly, G.R., 1999. Stratigraphy of the west-central part of the Barberton Greenstone
673 Belt, South Africa. In: Lowe, D.R., Byerly, G.R. (Eds.), Geological Evolution of the Barberton
674 Greenstone Belt. Geol. Soc. Am. Spec. Paper 329, 1-36.

675 Maya, J.M., Bhutani, R., Balakrishnan, R., Sandhya, S.R., 2016. Petrogenesis of 3.15 Ga old
676 Banasandra komatiites from the Dharwar craton, India: Implications for early mantle heterogeneity.
677 Geosci. Frontiers 8, 467-481.

678 Meissner, F., Schmidt-Ott, W.-D., Ziegeler, L. 1987. Half-life and α-ray energy of ^{146}Sm. Z. Phys. A
679 327, 171-174.

680 Moyen, J.-F., 2011. The composite Archaean grey gneisses: petrological significance, and evidence
681 for a non-unique tectonic setting for Archaean crustal growth. Lithos 123, 21-36.

682 Moyen, J.F., Martin, H., 2012. Forty years of TTG research. Lithos 148, 312-336.

683 Murphy, R.C.L., 2015. Stabilising a craton: The origin and emplacement of the 3.1 Ga Mpuluzi
684 Batholith. PhD thesis, Macquarie University, Sydney, http://hdl.handle.net/1959.14/1069283.

685 Nutman, A.P., McGregor, V.R., Friend, C.R.L., Bennett, V.C., Kinny, P.D., 1996. The Itsaq Gneiss
686 Complex of southern West Greenland; the world's most extensive record of early crustal evolution
687 (3900-3600 Ma). Precambrian Res. 78, 1-397.

688 O'Neil, J., Boyet, M., Carlson, R.W., Paquette, J.-L., 2013. Half a billion years of reworking of
689 Hadean mafic crust to produce the Nuuvuagittuq Eoarchean felsic crust. Earh Planet, Sci. Lett. 379,
690 13-25.

691 O'Neil, J., Carlson, R.W., 2017. Building Archean cratons from Hadean mafic crust. Science 355,
692 1199-1202.

693 O'Neil, J., Carlson, R.W., Francis, D., Stevenson, R.K., 2008. Neodymium-142 evidence for hadean
694 mafic crust. Science 321, 1828-1831.

695 O'Neil, J., Carlson, R.W., Paquette, J.-L., Francis, D., 2012. Formation age and metamorphic history
696 of the Nuvvuagittuq greenstone belt. Precambrian Res. 220-221, 23-44.

697 O'Neil, J., Rizo, H., Boyet, M., Carlson, R.W., Rosing, M.T., 2016. Geochemistry and Nd isotopic
698 characteristics of Earth´s Hadean mantle and primitive crust. Earth Planet. Sci. Lett. 442, 194-205.

699 Puchtel, I.S., Blichert-Toft, J., Touboul, M., Horan, M.F., Walker, R.J., 2016. The coupled ^{182}W-^{142}Nd
700 record of early terrestrial mantle differentiation. Geochem. Geophys. Geosyst. 17,
701 doi:10.1002/2016GC006324.

702 Puchtel, I.S., Blichert-Toft, J., Touboul, M., Walker, R.J., Byerly, G.R., Nisbet, E.G., Anhaeusser,
703 C.R., 2013. Insights into early Earth from Barberton komatiites: evidence from lithophile isotope and
704 trace element systematics. Geochim. Cosmochim. Acta 108, 63-90.

705 Rizo, H., Boyet, M., Blichert-Toft, J., O'Neil, J., Rosing, M.T., Paquette, J.-L., 2012. The elusive
706 Hadean enriched reservoir revealed by ^{142}Nd deficits in Isua Archean rocks. Nature 491, 96-100.

707 Rizo, H., Boyet, M., Blichert-Toft, J., Rosing, M.T., 2011. Combined Nd and Hf isotope evidence for
708 deep-seated source of Isua lavas. Earth Planet. Sci. Lett. 312, 267-279.

709 Rizo, H., Boyet, M., Blichert-Toft, J., Rosing, M.T., 2013. Early mantle dynamics inferred from ^{142}Nd
710 variations in Archean rocks from southwest Greenland. Earth Planet. Sci. Lett. 377, 324-335.

711 Robin-Popieul, C.C.M., Arndt, N.T., Chauvel, C., Byerly, G.R., Sobolev, A.V., Wilson, A., 2012. A
712 new model for Barberton komatiites: deep critical melting with high melt retention. J. Pet. 53, 2191-
713 2229.

714 Roerdink, D.L., Mason, P.R.D., Whitehouse, M.J., Brouwer, F.M., 2016. Reworking of atmospheric
715 sulfur in a Paleoarchean hydrothermal system at Londozi, Barberton Greenstone Belt, Swaziland.
716 Precambrian Res. 280, 195-204.

717 Roth, A.S.G., Bourdon, B., Mojzsis, S.J., Touboul, M., Sprung, P., Guitreau, M., Blichert-Toft J.,
718 2013. Inherited ^{142}Nd anomalies in Eoarchean protoliths. Earth Planet. Sci. Lett. 361, 50-57.

719 Roth, A.S.G., Bourdon, B., Mojzsis, S.J., Rudge, J.F., Guitreau, M., Blichert-Toft, J., 2014a.
720 Combined ^{147,146}Sm-^{143,142}Nd constraints on the longevity and residence time of early terrestrial crust.
721 Geochem., Geophys., Geosyst. 15, 2329-2345.

722 Roth, A.S.G., Scherer, E.E., Maden, C., Mezger, K., Bourdon, B., 2014b. Revisiting the ^{142}Nd deficits
723 in the 1.48 Ga Khariar alkaline rocks, India. Chem. Geol. 386, 238-248.

724 Schoene, B., De Wit, M.J., Bowring, S.A., 2008. Mesoarchean assembly and stabilization of the
725 eastern Kaapvaal Craton: a structural-thermochronological perspective. Tectonics 27, TC5010.

726 Schoene, B., Dudäs, F.O.L., Bowring, S.A., de Wit, M.J., 2009. Sm-Nd isotopic mapping of
727 lithospheric growth and stabilization in the eastern Kaapvaal craton. Terra Nova 21, 219-228.

728 Sossi, P.A., Eggins, S.M., Nesbitt, R.W., Nebel, O., Hergt, J.M., Campbell, I.H., O´Neill, H.S.C., Van
729 Kranendonk, M., Davies, D.R., 2016. Petrogenesis and geochemistry of Archean komatiites. J. Pet. 57,
730 147-184.

731 Suhr, N., Hoffmann, J.E., Kröner, A., Schröder, S., 2015. Archaean granulite-facies paragneisses from
732 central Swaziland: inferences on Palaeoarchaean crustal reworking and a complex metamorphic
733 history. J. Geol. Soc. Lond. 172, 139-152.

734 Tang, M., Wang, X.-L., Shu, X.-J., Wang, D., Yang, T., Gopon, P., 2014. Hafnium isotopic
735 heterogeneity in zircons from granitic rocks: geochemical evalution and modeling of "zircon effect" in
736 crustal anatexis. Earth Planet. Sci. Lett. 389, 188-199.

737 Taylor, J., Stevens, G., Buick, I.S., Lana, C., 2012. Successive mid-crustal, high-grade metamorphic
738 events prove insight into Mid-Archean mountain-building along the SE margin of the proto-Kaapvaal
739 craton. Geol. Soc. Am. Bull. 124, 1191-1211.

740 Van Kranendonk, M.J., Hickman, A., Smithies, R.H., 2007. Paleoarchean development of a
741 continental nucleus: the East Pilbara Terrane of the Pilbara Craton, Western Australia. In: Van
742 Kranendonk, M.J., Smithies, R.H., Bennet, V. (Eds.), Earth's Oldest Rocks. Elsevier, Amsterdam,
743 Developments in Precambrian Geology 15, 307-337.

744 Van Kranendonk, M.J., Kröner, A., Hegner, E., Connelly, J., 2009. Age, lithology and structural
745 evolution of the c. 3.53 Ga Theespruit Formation in the Tjakastad area, southwestern Barberton
746 Greenstone Belt, South Africa, with implications for Archean tectonics. Chem. Geol. 261, 115-139.

747 Van Kranendonk, M.J., Smithies, R.H., Griffin, W.L., Huston, D.L., Hickman, A.H., Champion, D.C.,
748 Anhaeusser, C.R., Pirajno, F., 2014. Making it thick: a volcanic plateau origin of Palaeoarchean
749 continental lithosphere of the Pilbara and Kaapvaal cratons. J. Geol. Soc. Lond. Special Publications
750 389, http://dx.doi.org/10.1144/SP389.12.

751 Van Schijndel, V., Stevens, G., Zeh, A., Frei, D., Lana, C. 2017. Zircon geochronology and Hf
752 isotopes of the Dwalile Supracrustal Suite, Ancient Gneiss Complex, Swaziland: Insights into the
753 diversity of Palaeoarchaean source rocks, depositional and metamorphic ages. Precambrian Res. 295,
754 48-66.

755 Wilde, S.A., Valley, J.W., Peck, W.H., Graham, C.M., 2001. Evidence from detrital zircons for the
756 existence of continental crust and oceans on the Earth 4.4 Gyr ago. Nature 409, 175-178.

757 Zeh, A., Gerdes, A., Millonig, L., 2011. Hafnium isotope record of the Ancient Gneiss Complex,
758 Swaziland, southern Africa; evidence for Archaean crust–mantle formation and crust reworking
759 between 3.66 and 2.73 Ga. J. Geol. Soc. Lond. 168, 1-11.

Table 1: Measured ^{142}Nd data for granitoids and (ultra-)mafic rocks from the Ancient Gneiss Complex and Barberton Greenstone Belt.

Sample	Age	$^{142}Nd/^{144}Nd$	±2s.e. on last decimals place	$\mu^{142}Nd$ (ppm)	±2s.e. (ppm)	$^{143}Nd/^{144}Nd$	±2s.e. on last decimals place	ε143Nd*	$^{145}Nd/^{144}Nd$	±2s.e. on last decimals place	$\mu^{145}Nd$ (ppm)	±2s.e. (ppm)	$^{146}Nd/^{144}Nd$	±2s.e. on last decimals place	$^{148}Nd/^{144}Nd$	±2s.e. on last decimals place	$\mu^{148}Nd$ (ppm)	±2s.e. (ppm)	$^{150}Nd/^{144}Nd$	±2s.e. on last decimals place	$\mu^{150}Nd$ (ppm)	±2s.e. (ppm)
Samples 1. analytical session																						
AGC372	3552	1.141832	4	-5.6	3.7	0.510649	2	-0.6	0.348406	1	12.6	3.4	0.722331	100	0.241581	2	-7.5	6.2	0.236448	2	-35.7	7.9
BA156	3530	1.141839	4	0.0	3.2	0.512711	2	0.8	0.348404	1	7.0	2.8	0.723225	60	0.241581	1	-5.8	5.0	0.236450	2	-26.4	7.2
AGC75 #R1	3478	1.141833	4	-4.8	3.9	0.510531	2		0.348403	1	2.8	3.7	0.721429	24	0.241580	1	-13.0	6.0	0.236449	2	-30.0	8.1
AGC75 #R2	3478	1.141832	4	-5.9	3.7	0.510532	2		0.348402	1	0.7	3.3	0.722741	53	0.241580	1	-12.3	5.9	0.236449	2	-29.5	7.8
AGC75 average				-5.4				0.2														
AGC352	3442	1.141830	4	-7.9	3.1	0.510989	2	1.1	0.348403	1	4.1	2.9	0.722696	60	0.241581	1	-6.9	5.1	0.236449	2	-33.0	7.0
AGC222	3400	1.141840	3	0.6	3.0	0.512396	2	1.6	0.348403	1	3.9	2.9	0.723633	87	0.241582	1	-2.3	5.3	0.236451	2	-25.0	6.8
AGC368	3261	1.141835	3	-3.3	2.7	0.510369	2	-1.0	0.348403	1	3.8	2.8	0.723632	15	0.241579	1	-17.1	4.7	0.236448	1	-36.4	6.3
AGC445	3216	1.141833	4	-5.4	3.2	0.510727	2	-1.1	0.348405	1	7.6	3.1	0.722131	93	0.241580	1	-11.5	5.3	0.236446	2	-44.3	7.2
BHVO2		1.141842	5	2.4	3.9	0.512976	2		0.348404	1	6.5	3.9	0.721600	59	0.241582	2	-3.9	6.6	0.236446	2	-43.4	8.6
Samples 2. analytical session																						
AGC 150b #R1	3661	1.141827	3	0.2	2.8	0.510981	1		0.348400	1	2.6	2.8	0.721711	66	0.241577	1	-2.2	4.5	0.236448	1	-8.7	6.2
AGC 150b #R2	3661	1.141825	4	-1.8	3.1	0.510981	2		0.348400	1	3.0	2.8	0.723316	24	0.241578	1	4.2	5.0	0.236452	2	5.6	6.9
AGC 150b average				-0.8				0.7														
KS-BA189	3553	1.141827	6	0.4	5.0	0.511444	3	1.1	0.348401	2	5.4	5.0	0.721973	47	0.241577	2	0.4	8.7	0.236451	3	1.7	11.1
AGC 370	3552	1.141822	4	-4.2	3.8	0.510128	2	1.4	0.348401	1	6.4	3.5	0.721285	94	0.241577	1	-0.6	6.1	0.236448	2	-11.4	8.5
BA132 #R1	3509	1.141824	4	-2.6	3.3	0.510621	2		0.348400	1	3.3	2.9	0.720851	52	0.241576	1	-2.4	5.0	0.236448	2	-10.2	7.3
BA132 #R2	3509	1.141823	4	-3.8	3.9	0.510621	2		0.348402	1	9.0	3.4	0.722296	19	0.241576	1	-4.5	5.9	0.236447	2	-15.7	8.3
BA132 average				-3.2																		
ZA32a	3480	1.141821	4	-5.4	3.7	0.512140	2	0.3	0.348402	1	7.5	3.1	0.722807	176	0.241577	1	1.2	5.5	0.236446	2	-17.4	7.7
BA128	3465	1.141827	3	0.1	2.6	0.511125	1	0.2	0.348400	1	2.2	2.9	0.723051	33	0.241579	1	8.0	4.1	0.236453	1	10.9	4.2
AGC350 #R1	3455	1.141825	5	-1.9	4.5	0.511909	2		0.348401	1	4.4	3.9	0.720526	68	0.241578	2	2.5	7.4	0.236450	2	-3.2	10.2
AGC350 #R2	3455	1.141829	5	2.1	4.6	0.511913	2		0.348400	1	1.2	3.4	0.722572	32	0.241576	1	-5.7	5.9	0.236450	2	-0.8	7.7
AGC350 #R3	3455	1.141825	5	-2.0	4.0	0.511911	2		0.348400	1	3.5	3.7	0.724003	34	0.241578	2	4.0	6.7	0.236450	2	-2.0	9.2
AGC350 average				-0.6				0.5														
AGC50 #R1	3458	1.141821	4	-5.4	3.9	0.511791	2		0.348401	1	4.6	3.9	0.720716	47	0.241577	2	-0.6	6.6	0.236447	2	-13.2	8.8
AGC50 #R2	3458	1.141819	4	-6.7	3.7	0.511789	2		0.348400	1	1.9	3.4	0.722796	50	0.241576	1	-2.4	6.0	0.236445	2	-24.8	7.4
AGC50 average				-6.1																		
AGC 45	3445	1.141820	4	-6.2	3.1	0.512141	2	0.0	0.348399	1	-0.1	2.7	0.720788	89	0.241575	1	-7.4	4.9	0.236449	1	-7.1	6.3
AGC473	3241	1.141830	3	3.0	3.0	0.510548	1	-1.0	0.348401	1	4.0	2.2	0.722943	45	0.241577	1	-2.1	3.9	0.236449	1	-6.3	5.5

* Calculated with $^{147}Sm/^{144}Nd$ and initial $^{143}Nd/^{144}Nd$ of published isotope data. For published $^{147}Sm/^{144}Nd$ and initial $^{143}Nd/^{144}Nd$ isotope data please refer to Table S1 of the supplementary material.
#R1, #R2 means run 1, run 2

Sample	$^{142}Nd/^{144}Nd$	±2s.e. on last decimals place	$\mu^{142}Nd$ (ppm)	±2s.e. (ppm)	$^{143}Nd/^{144}Nd$	±2s.e. on last decimals place	ε143Nd*	$^{145}Nd/^{144}Nd$	±2s.e. on last decimals place	$\mu^{145}Nd$ (ppm)	±2s.e. (ppm)	$^{146}Nd/^{144}Nd$	±2s.e. on last decimals place	$^{148}Nd/^{144}Nd$	±2s.e. on last decimals place	$\mu^{148}Nd$ (ppm)	±2s.e. (ppm)	$^{150}Nd/^{144}Nd$	±2s.e. on last decimals place	$\mu^{150}Nd$ (ppm)	±2s.e. (ppm)
Terrestrial stds 1. analytical session																					
JNdi-1	1.141840	8	1.1	3.3	0.512103	3		0.348402	2	-0.5	5.5	0.723837	17	0.241582	2	-3.9	10.3	0.236455	3	-4.5	14.2
JNdi-1	1.141835	6	-3.8	2.7	0.512101	2		0.348402	1	0.5	4.1	0.722755	88	0.241583	2	1.4	7.7	0.236457	2	4.3	10.3
JNdi-1	1.141836	6	-2.5	2.8	0.512103	3		0.348402	2	-0.9	5.2	0.722290	65	0.241583	2	1.6	8.6	0.236459	3	10.6	11.7
JNdi-1	1.141836	7	-2.2	3.1	0.512103	3		0.348402	2	1.4	5.6	0.722718	15	0.241583	2	-0.5	9.6	0.236456	3	-3.3	14.0
JNdi-1	1.141843	8	3.6	3.7	0.512102	4		0.348402	2	0.8	6.0	0.722830	62	0.241583	3	-1.0	10.6	0.236457	3	1.8	14.8
JNdi-1	1.141839	8	0.5	3.6	0.512101	3		0.348401	2	-2.2	5.7	0.721677	76	0.241582	2	-3.0	10.0	0.236455	3	-7.9	14.5
JNdi-1	1.141841	7	1.5	3.2	0.512104	4		0.348402	2	0.6	5.9	0.722316	95	0.241582	2	-5.2	10.0	0.236455	3	-4.1	14.2
JNdi-1	1.141837	17	-1.6	7.2	0.512101	7		0.348400	4	-4.5	12.3	0.721402	110	0.241585	6	9.7	24.6	0.236458	8	7.0	32.8
JNdi-1	1.141837	7	-1.4	3.3	0.512104	4		0.348401	2	-2.2	7.2	0.722926	35	0.241582	3	-2.4	12.0	0.236456	4	-1.7	16.0
JNdi-1	1.141841	7	1.7	3.0	0.512104	3		0.348402	2	1.4	5.6	0.722075	69	0.241584	2	3.5	10.0	0.236457	3	2.9	14.6
JNdi-1	1.141839	7	0.3	3.1	0.512104	4		0.348402	2	0.1	6.7	0.722491	12	0.241583	3	2.3	11.2	0.236458	4	4.6	15.3
JNdi-1	1.141842	7	2.9	3.1	0.512104	3		0.348403	2	1.8	5.6	0.723389	98	0.241583	3	-0.4	10.6	0.236455	3	-6.4	13.9
JNdi-1	1.141839	9	0.0	3.8	0.512104	5		0.348403	3	3.5	8.3	0.722572	61	0.241584	3	3.5	13.5	0.236459	5	12.5	19.8
JNdi-1 average 1. session	1.141839	5	0.0	4.4 (2s.d.)																	
Terrestrial stds 2. analytical session																					
JNdi-1	1.141823	6	-3.4	5.0	0.512107	3		0.348399	2	-0.7	4.4	0.720617	65	0.241575	2	-9.3	7.7	0.236446	3	-19.7	10.8
JNdi-1	1.141823	3	-3.5	3.0	0.512107	2		0.348398	1	-4.8	2.6	0.720659	61	0.241574	1	-11.2	4.9	0.236445	2	-24.2	6.8
JNdi-1	1.141828	4	0.5	3.1	0.512105	2		0.348402	1	8.8	2.9	0.720515	32	0.241578	1	5.9	5.0	0.236454	2	15.3	6.6
JNdi-1	1.141824	3	-2.7	2.8	0.512103	1		0.348402	1	9.2	2.3	0.721589	24	0.241579	1	7.7	4.0	0.236454	1	16.1	5.5
JNdi-1	1.141823	4	-3.5	3.2	0.512104	2		0.348399	1	-0.1	2.5	0.720704	48	0.241578	1	2.4	4.9	0.236451	2	4.3	6.9
JNdi-1	1.141826	3	-0.8	2.9	0.512105	1		0.348398	1	-2.2	2.4	0.723311	67	0.241577	1	1.4	4.6	0.236451	1	1.8	6.1
JNdi-1	1.141826	3	-1.0	2.5	0.512106	1		0.348399	1	-1.5	2.2	0.720810	55	0.241576	1	-5.0	3.9	0.236449	1	-5.0	5.3
JNdi-1	1.141827	3	0.3	2.4	0.512106	1		0.348399	1	-0.1	2.1	0.723915	74	0.241576	1	-2.8	3.6	0.236449	1	-4.4	5.2
JNdi-1	1.141828	3	0.7	3.0	0.512106	2		0.348399	1	-0.1	2.8	0.721511	51	0.241577	1	1.3	4.7	0.236451	2	2.0	6.7
JNdi-1	1.141828	4	0.9	3.2	0.512105	2		0.348398	1	-4.1	2.9	0.723244	48	0.241578	1	5.0	5.2	0.236453	2	10.6	6.8
JNdi-1	1.141830	3	2.7	2.8	0.512106	1		0.348400	1	1.4	2.4	0.721490	65	0.241578	1	3.6	4.2	0.236450	1	-1.9	5.9
JNdi-1	1.141830	3	2.7	2.8	0.512106	1		0.348400	1	1.4	2.4	0.721490	65	0.241578	1	3.6	4.2	0.236450	1	-1.9	5.9
JNdi-1	1.141829	3	2.2	3.1	0.512107	2		0.348399	1	-0.8	2.8	0.723453	52	0.241577	1	-0.3	5.1	0.236451	2	4.4	7.1
JNdi-1	1.141828	5	0.5	4.0	0.512108	2		0.348399	1	-1.6	3.5	0.721598	56	0.241578	1	4.0	5.8	0.236452	2	8.2	8.6
JNdi-1	1.141828	4	1.0	3.7	0.512108	2		0.348399	1	-0.1	3.2	0.723597	36	0.241579	1	7.1	5.8	0.236454	2	15.9	7.3
JNdi-1	1.141828	5	1.2	4.0	0.512108	2		0.348397	1	-5.0	3.7	0.721057	50	0.241575	2	-9.0	6.4	0.236448	2	-10.0	8.7
JNdi-1	1.141829	4	2.1	3.7	0.512110	2		0.348399	1	0.1	3.0	0.724330	45	0.241576	1	-4.6	5.2	0.236448	2	-11.6	7.6
JNdi-1 average 2. session	1.141827	5	0.0	4.3 (2s.d.)																	

Table S1: Summary of major and trace element as well as ^{147}Sm-^{143}Nd and ^{176}Lu-^{176}Hf isotope data.

	Ancient Gneiss Complex											Barberton Greenstone Belt						
Sample	**AGC 150b[a]**	**AGC 370[a]**	**AGC 75[b]**	**AGC 50[c]**	**AGC 350[#]**	**AGC 45[c]**	**AGC 352[b]**	**AGC 222[b]**	**AGC 368[#]**	**AGC 473[#]**	**AGC 445[#]**	**KS-BA 189[#]**	**error (%)**	**AGC 372[d]**	**BA 156[#]**	**BA 132[#]**	**ZA-32a[#]**	**BA 128[#]**
Lithology	grey gneiss	tonalite	tonalitic gneiss	meta-komatiite	foliated metagabbro	amph. - komatiitic basalt	grey gneiss	amphibolite	granodiorite	throndhjemitic gneiss	grey gneiss	tholeiitic basalt		felsic volcanic rock	amph. - tholeiitic pillow basalt	throndhjemite	tholeiite	tonalitic gneiss
Age (Ma)	3661	3552	3478	3458	3455	3445	3442	>3400	3261	3241	3216	3553		3552	3530	3509	3480	3465
Formation	Gneiss (Piggs Peak)	Piggs Peak	Tsawela Gneiss	Dwalile	Mtimane River	Dwalile	Ngwane Gneiss	Kubuta	Usutu Suite	Dwalile	Piggs Peak	Sandspruit Fm		Theespruit Fm.	Theespruit Fm.	Steynsdorp Pluton	Komati Fm.	Theespruit Pluton
Major elements (%)																		
SiO2	69.7	78.1	63.5	49.6	55.4	49.1	70.1	46.8	64.9	68.7	58.0	52.1		62.80	53.7	71.9	53.2	69.1
TiO2	0.390	0.160	0.577	0.463	1.08	0.775	0.493	1.66	0.790	0.487	1.15	0.500		0.80	0.964	0.295	0.771	0.27
Al2O3	12.6	12.4	15.9	4.56	15.0	9.76	14.7	14.6	16.7	16.4	18.4	13.8		17.04	13.9	15.3	12.1	15.0
Fe2O3	5.69	1.47	5.71	6.14	9.89	3.18	4.19	15.4	5.45	3.18	7.46	10.6		5.76	11.8	2.59	11.6	2.95
FeO				7.04		9.98												
MnO	0.0700	0.0400	0.0911	0.252	0.131	0.245	0.0604	0.201	0.0559	0.0405	0.0813	0.163		0.08	0.175	0.0509	0.193	0.0297
MgO	2.43	0.450	3.07	23.3	6.38	15.3	1.48	7.16	1.59	0.862	1.93	10.01		2.05	6.20	0.570	8.94	1.35
CaO	1.41	1.22	5.35	8.40	7.00	9.80	2.49	10.9	4.25	2.96	5.76	10.35		4.91	10.8	2.24	9.65	2.79
K2O	2.54	1.64	1.50	0.0315	1.46	0.0917	1.44	2.11	1.19	1.76	1.59	0.537		3.17	0.0366	2.10	0.165	1.47
Na2O	1.71	4.78	4.14	0.126	3.49	1.35	4.92	0.803	4.83	5.50	5.31	1.81		3.16	2.39	4.94	3.27	5.35
P2O5	0.0900	0.0400	0.121	0.0526	0.158	0.122	0.131	0.301	0.259	0.152	0.345	0.0799		0.24	0.0870	0.0611	0.0906	0.0892
Trace elements (ppm)				*														
Li	241		45.1		17.2		14.0	12.2		63.4	178				7.55	111	5.76	41.0
Sc	4.82	1.72	12.2	16.6	25.2	25.5	5.91	41.0		2.10	3.27	30.3	6		35.9	1.86	27.1	3.47
V	21.6		96.3	116	152	225	54.8	404		27.2	104	165	4		326	14.9	218	62.5
Cr	17.5	6.70	73.4	1891	205	1765	28.8	127		7.97	4.10				147	5.16	691	438
Co	11.1	4.32	21.0		41.6	90.0	10.6	62.1		5.23	15.7	58.6	3		46.1	3.00	52.1	7.76
Ni	12.2	18.3	60.4	1231	139	403	17.9	127		3.80	5.23				101	4.09	173	39.8
Cu	109		37.9	54.8	25.3	51.0	3.09	100		10.5	37.9	67.4	7		155	8.16	123	4.86
Zn	164		65.9	86.0	125	121	77.7	121		68.4	128	74.5	19		83.5	48.5	74.4	50.0
Ga	23.5		18.6		22.8		20.7	18.8		21.0	22.9	12.7	4		15.2	20.2	11.4	18.2
Rb	229	61.5	76.9	4.98	56.3	10.0	38.5	69.4		28.8	50.6				0.416	33.0	2.71	53.1
Sr	121	215	393	24.6	418	23.0	595	143		367	499	182	6		116	312	198	574
Y	59.4	4.5	15.5	8.57	39.5	22.0	16.2	27.4		11.2	11.7	16.7	8		23.2	13.4	18.5	5.93
Zr	340	134	147	40.4	139	66.0	176			183	218	65.5	7		62.5	170	66.5	131
Nb	33.8	6.57	6.95	2.02	9.34	5.00	6.95	3.90		8.85	9.25	3.10	14		2.65	9.20	3.66	4.68
Mo			1.19		0.170		0.254	0.304		0.243	0.565	0.513	6		0.272	0.117	0.336	
Cd			0.124		0.200		0.132	0.167		0.157	0.325	0.0949	17			0.155	0.111	
Sn					1.69		1.55	0.370		1.77	3.52	0.568	8		0.164	0.184	0.623	
Sb			0.0612		0.0400		0.0689	0.0691		0.0367	0.0442				0.220	0.295	0.0631	
Cs	21.2		1.19	2.16	0.850	3.91	0.760	2.67		2.46	13.8				0.116	6.38	0.272	2.58
Ba	537	633	296	6.79	234		376	45.0		384	446	89.1	5		24.3	479	53.9	322
La	51.2	20.8	28.2	3.84	12.2	4.06	20.1	5.30		28.8	37.3	8.71	4		3.28	19.6	4.40	9.02
Ce	93.8	40.8	56.9	9.05	32.7	10.8	36.5	13.8		37.8	47.6	18.0	4		8.87	25.4	11.34	16.2
Pr	11.2	3.49	6.45	1.24	4.97	1.72	4.65	2.06		6.20	9.21	2.22	4		1.38	4.11	1.66	2.00
Nd	41.8	12.2	24.0	5.56	24.1	8.19	18.1	10.2		23.2	37.5	9.08	3		7.21	15.2	7.94	8.20
Sm	8.88	1.55	4.16	1.50	6.54	2.36	3.73	3.06		4.02	6.80	2.18	7		2.38	2.91	2.29	1.82
Eu	1.37	0.760	1.14	0.404	1.66	0.700	1.04	1.25		1.07	1.90	0.600	7		0.887	0.735	0.756	0.64
Gd	9.15	1.22	3.77	1.70	7.02	2.82	3.37	4.01		3.14	5.26	2.52	6		3.17	2.58	2.84	1.59
Tb	1.55	0.150	0.492	0.269	1.15	0.490	0.510	0.690		0.391	0.626	0.405	7		0.570	0.390	0.496	0.21
Dy	9.88	0.880	2.70	1.60	7.10	3.42	2.96	4.58		1.92	2.70	2.71	16		3.90	2.29	3.28	1.15
Ho	2.04	0.160	0.525	0.321	1.41	0.760	0.580	0.970		0.337	0.390	0.586	7		0.836	0.454	0.688	0.21
Er	5.76	0.440	1.45	0.916	3.81	2.3	1.60	2.72		0.865	0.857	1.69	6		2.38	1.29	1.94	0.57
Tm	0.83	0.070	0.221	0.130	0.54	0.311	0.229	0.406		0.119	0.103	0.255	7		0.364	0.193	0.290	0.0810
Yb	5.24	0.460	1.45	0.826	3.39	1.87	1.49	2.68		0.725	0.611	1.68	7		2.43	1.30	1.92	0.51
Lu	0.760	0.080	0.227	0.117	0.488	0.360	0.222	0.418		0.101	0.0844	0.251	9		0.356	0.221	0.298	0.0720
Hf	9.65	3.39	3.64	0.975	3.15	1.91	4.47	2.02		4.48	5.23	1.78	4		1.61	4.34	1.63	3.23
Ta	2.54	0.420	0.459	0.138	0.483	0.263	0.544	0.230		0.786	0.486	0.202	11		0.165	0.921	0.216	0.400
W			0.142		0.250		0.144	2.306		0.120	0.293	0.294	10		0.127	0.392	0.105	
Tl			0.39		0.280		0.285	0.331		0.402	0.631				0.0361	0.336	0.0280	
Pb	9.60	10.6	6.03	0.551	3.94	0.379	4.78	5.17		9.87	9.69	2.43	7		0.552	6.795	0.707	7.33
Th	14.5	3.00	4.01	0.520	0.680	0.476	3.86	0.440		4.71	4.75	1.43	7		0.252	3.73	0.403	1.88
U	3.73	0.980	0.743	0.135	0.260	0.125	0.625	0.153		0.838	2.55	0.203	7		0.0868	0.705	0.101	
Isotopic composition				*				#										
Sm (ppm)	9.01	1.97	3.80	1.36	6.09	2.21	3.71	2.85	4.90	4.93	6.80	1.99		6.16	2.14	3.44	2.10	1.85
Nd (ppm)	42.5	13.7	21.8	5.16	22.4	7.68	18.4	9.41	30.2	30.5	37.5	8.42		32.8	6.54	18.9	7.31	8.67
$^{147}Sm/^{144}Nd$	0.1280	0.0868	0.1050	0.1592	0.1642	0.1743	0.1220	0.1830	0.0979	0.0978	0.1095	0.1426		0.1135	0.1983	0.1097	0.1738	0.1290
$^{143}Nd/^{144}Nd_0$	0.511019	0.510137	0.510548	0.511775	0.511922	0.512138	0.511004	0.512410	0.510422	0.510545	0.510736	0.511431		0.510660	0.512728	0.510609	0.512134	0.511105
±	14	13	11	9	10	9	16	8	8	6	7	7		9	7	13	8	20
$\varepsilon^{143}Nd(t)$	0.72	1.44	0.22	-0.30	0.50	0.05	1.15	1.62	-1.85	-1.00	-1.10	1.13		-0.62	0.87	-0.40	0.29	0.20
Lu (ppm)	0.778	0.0988	0.216	0.120	0.488	0.289	0.222	0.414	0.157	0.111	0.0840	0.257		0.393	0.368	0.221	0.295	0.0766
Hf (ppm)	8.39	4.47	3.64	0.952	3.12	1.74	4.47	2.22	7.18	4.62	5.23	1.77		5.55	1.69	4.27	1.70	3.68
$^{176}Lu/^{177}Hf_0$	0.0132	0.00314	0.00843	0.0179	0.0222	0.0236	0.00705	0.0265	0.0031	0.00343	0.00229	0.0206		0.0100	0.0310	0.00735	0.0246	0.00296
$^{176}Hf/^{177}Hf_0$	0.281410	0.280755	0.281164	0.281786	0.282105	0.282186	0.281174	0.282472	0.280896	0.280894	0.280854	0.281991		0.281139	0.282689	0.281014	0.282255	0.280738
±	7	7	5	22	5	10	6	7	7	7	11	11		6	6	5	5	7
εHf(t)	2.53	2.09	2.41	1.70	2.80	2.33	5.39	6.00	0.92	-0.30	0.23	3.50		-1.07	2.98	-4.30	2.60	0.10
Sm/Nd	0.212	0.143	0.174	0.264	0.272	0.288	0.202	0.302	0.162	0.162	0.181	0.236		0.188	0.328	0.182	0.288	0.213

[a] **Kröner et al. 2014**
[b] **Hoffmann et al. 2016**
[c] **Kröner & Tegtmeyer 1994**
[d] **Kröner et al. 2013**
[e] **Sample BA 115 from Kröner et al. 2016**
* **AGC 50: TE and Isotopes by Hoffmann et al in prep.**
[#] **this study, ages: pers. comm. A. Kröner 2016**

Supplementary information S2: Sample digestion and chemical separation for $^{142}Nd/^{144}Nd$ analyses

Sample powders were digested in a mixture of concentrated HF-HNO_3 in Parr® pressure vessels for 48 hours and dried down with one additional milliliter of $HClO_4$. Subsequently, 5 ml conc. HNO_3 was added to the samples and dried down immediately. After evaporation, the samples were dissolved in 6 ml 6 N HCl overnight. After full equilibration was reached, the samples were evaporated to dryness.

For purifying Nd from the whole rock sample solutions, four chemical separations were implemented. The first separation was performed on ca. 20 cm long and 6 mm wide Teflon columns filled with AG-50W-x8 200-400 µm mesh resin. Samples were loaded in 2.5 N HCl. Major elements were eluted with 44 ml of 2.5 N HCl and heavy REE were eluted in 10 ml 4 N HCl. The remaining REE fraction was collected in 29 ml of 6 N HCl and subsequently dried down. In a second stage, the REE fraction was diluted in 0.2 ml of a mixture of 10 N HNO_3 and 20 mM $NaBrO_3$ and loaded on 12 mm long and 7 mm wide PET columns filled with 1 ml of Eichrom Ln-Spec 50-100 µm resin to remove Ce from the REE fraction. Details are given in Tazoe et al. (2007). After elution of the REE fraction, a mixture of 6 N HCl and H_2O_2 was added to the columns to reduce Ce and ensure that no Ce^{4+} is present. This chemical separation was done twice to reduce the Ce content to negligible levels. In a third step 6 cm long and 4 mm wide quartz columns filled with 300 mg of Eichrom Ln-Spec 25-50 µm resin were used to purify the Nd from all other REE. In order to do that, the samples were loaded in 0.2 ml of 0.2 N HCl. The light REE were eluted with 10.5 ml of 0.2 N HCl. Subsequently, the Nd fraction was collected in 3 ml of 0.25 N HCl. However, after checking the elemental content in the samples at the ICP-MS, some samples still showed comparatively high Ba concentrations. Consequently, a fourth separation was applied to remove Ba from the samples. For this separation, columns filled with 1 ml of AGW50-X8 200-400 µm mesh resin were used. The samples were loaded in 2.5 N HCl. The Ba was eluted with 2 N HNO_3 and the pure Nd fraction was subsequently collected in 6 N HCl. The total procedural blank determined by ICP-MS for Nd is 300 pg, The blank contribution was negligible in comparison to the Nd fractions for analyzed samples (> 500 ng).

Tazoe H., Obata H. and Gamo T. (2007) Determination of cerium isotope ratios in geochemical samples using oxidative extraction technique with chelating resin. *J. Anal. At. Spectrom.* **22**, 616-622.

Supplement S3: Analytical methods BA 132, BA 156, ZA-32a, KS-BA 189, AGC 222, AGC 350, AGC 445, AGC 473

Samples BA 132, BA 156, KS-BA 189, ZA-32a, AGC 350, AGC 368, AGC 445, and AGC 473 were analyzed for their whole rock major element compositions by X-ray fluorescence spectrometry (XRF) on $Li_2B_4O_7$-flux fusion discs using a PANalytical Axios X-ray spectrometer at the University of Cologne, Germany (Table S1). The loss on ignition (LOI) for each sample was determined by baking 1 g of rock powder in a muffle type furnace at 1000°C for 24 hours.

Samples BA 132, BA 156, KS-BA 189, ZA-32a, AGC 350, AGC 445, and AGC 473 were also analyzed for their trace element compositions. Sample powders were digested in Parr® pressure vessels in concentrated HF-HNO_3 for 72 hours and dried down with adding one milliliter of $HClO_4$. Subsequently 2 ml concentrated HNO_3 was added to the samples and dried down immediately. After evaporation to dryness, the samples were diluted in 3 % HNO_3 for trace element analysis. Samples BA 132, BA 156, and ZA-32a were analyzed at the University of Kiel, Germany, using an AGLIENT 7500cs quadrupole inductively coupled plasma mass spectrometer (ICP-MS). The analytical procedures followed Garbe-Schönberg (1993). Sample KS-BA 189 was analyzed at the Freie Universität Berlin using a Thermo Finnigan Element XR ICP-MS. Samples were diluted by dilution factors of 14000 to 64000 depending on the trace element concentrations of the samples. In order to calibrate the measured intensities of the low, middle and high masses, an internal standard solution of 1 ppb Ge-In-Re was added to the end dilution. The end dilutions were measured against a calibration curve of several dilutions of BHVO-2 ranging from 11.000- to 600.000-fold dilutions that were also doped with a 1 ppb Ge-In-Re solution. Furthermore, two REE solutions containing 1 ppb and 0.4 ppb Ba, La, Ce, Pr, Nd, and Sm were measured along with the samples in order to determine the oxide ratio that was produced within the plasma during measurements. Following this procedure, relative errors for the REEs were usually around 5 % and range from 4 to 19 % for the HFSE, LILE, and Sc, V, Cr, Co, Ni, Cu, Zn (Table S1).

Samples BA 132, BA 156, KS-BA 189, ZA-32a, AGC 222, AGC 350, AGC 368, AGC 445, and AGC 473 were analyzed for their Hf and Nd isotopic compositions and Lu, Hf, Sm, Nd concentrations (Table S1). The analyses were obtained by isotope dilution using mixed ^{176}Lu-^{180}Hf and ^{149}Sm-^{150}Nd tracers following the protocols of Münker et al. (2001) and Weyer et al. (2002). Measurements were carried out using a Thermo Scientific Neptune multi-collector ICP-MS at the joint facility of the Cologne and Bonn universities (Germany), operated in static mode. Chemical separation of Hf and Nd followed the procedures outlined in Pin & Zalduegui (1997) and Münker et al. (2001). Reference materials AGV-2 and BHVO-2 were measured along with the samples to determine the accuracy of the results.

Measured values of ^{176}Hf/^{177}Hf and ^{143}Nd/^{144}Nd were corrected for mass fractionation using the exponential law and ^{179}Hf/^{177}Hf = 0.7325 and ^{146}Nd/^{144}Nd = 0.7219, respectively. All values are given relative to a ^{176}Hf/^{177}Hf of 0.282160 for the AMES solution that is isotopically indistinguishable

from JMC-475, and relative to a $^{143}Nd/^{144}Nd$ of 0.511859 for the La Jolla Nd standard. Samples were analyzed at the same concentrations as the standards, i.e. 24 ppb for AMES and 20 ppb for La Jolla. Typical external reproducibilities for Nd and Hf isotope measurements were ±0.3 ε-units. CHUR parameters used to calculate epsilon values are from Bouvier et al. (2008).

Figure S4: Evaluation of metamorphic disturbance. A) μ^{142}Nd anomalies vs. $(La/Yb)_{PMN}$. B) μ^{142}Nd anomalies vs. Pb content. No correlation can be observed between the μ^{142}Nd anomalies and elevated LREE or LILE. Consequently, we assume that metamorphic effects did not disturb the μ^{142}Nd anomalies of our AGC and BGB samples.